AGU PUBLICATIONS

Tectonics

RESEARCH ARTICLE
10.1002/2015TC004086

Key Points:
- Rapid Pliocene exhumation at syntaxis limited to temperatures of 300°C (~10 km)
- Applicability of cobbles for reconstruction of regional cooling histories
- Multidating of cobbles reveals cooling history of ice-covered rocks

Supporting Information:
- Text S1, Figures S1–S9, and Table S1
- Table S2
- Data Set S1
- Data Set S2

Correspondence to:
S. Falkowski,
sarah.falkowski@uni-tuebingen.de

Citation:
Falkowski, S., E. Enkelmann, K. Drost, J. A. Pfänder, K. Stübner, and T. A. Ehlers (2016), Cooling history of the St. Elias syntaxis, southeast Alaska, revealed by geochronology and thermochronology of cobble-sized glacial detritus, *Tectonics*, *35*, doi:10.1002/2015TC004086.

Received 20 NOV 2015
Accepted 1 FEB 2016
Accepted article online 5 FEB 2016

Cooling history of the St. Elias syntaxis, southeast Alaska, revealed by geochronology and thermochronology of cobble-sized glacial detritus

Sarah Falkowski[1], Eva Enkelmann[2], Kerstin Drost[1], Jörg A. Pfänder[3], Konstanze Stübner[1], and Todd A. Ehlers[1]

[1]Department of Geosciences, University of Tübingen, Tübingen, Germany, [2]Department of Geology, University of Cincinnati, Cincinnati, Ohio, USA, [3]Department of Geology, TU Bergakademie Freiberg, Freiberg, Germany

Abstract We investigate the spatiotemporal evolution of exhumation in the ice-covered St. Elias syntaxis area, southeast Alaska, using multiple thermochronometers and geochronometers from cobble-sized glacial detritus. Multiple thermochronometers reveal the cooling histories from 500 to 60°C of 27 glacially transported cobbles from the two largest catchments of the syntaxis. Cobble lithologies and 21 zircon U-Pb ages (~277–31 Ma) were examined to determine sample provenance. Furthermore, eight amphibole and seven biotite $^{40}Ar/^{39}Ar$ ages (~276–16 Ma and ~50–42 Ma, respectively), four zircon and six apatite (U-Th)/He ages (~35–4.8 Ma and ~4.2–0.6 Ma, respectively), and four apatite fission track ages (~17–1.6 Ma) were used to reconstruct the individual cobble cooling histories. An additional four bedrock samples from the Fairweather Range yielded three biotite $^{40}Ar/^{39}Ar$ ages between ~42 and 5 Ma. A compilation of published bedrock and new cobble cooling histories from the St. Elias Mountains and Fairweather Range reveals the regional Cenozoic cooling and exhumation history, emphasizing the position of the St. Elias syntaxis as a transitional zone between transpression and subduction settings. The new cobble and bedrock data indicate an onset of rapid exhumation at ~5 Ma that was limited in duration (2–3 Myr) and amount (~10 km) in the syntaxial region. This study also demonstrates the usefulness of cobbles for revealing thermal histories of otherwise inaccessible regions as cobble analysis combines advantages of bedrock and detrital thermochronology.

1. Introduction

Orogen syntaxes are sharp bends in orogenic belts [*Suess*, 1904]. Syntaxes constitute structurally complex zones that concentrate stresses and potentially influence far-field deformation [e.g., *Zeitler et al.*, 2001, 2014; *Mazzotti and Hyndman*, 2002; *Koons et al.*, 2010, 2013; *Bruhn et al.*, 2012]. Studying orogen syntaxes therefore improves the understanding of plate boundary deformation in these kinematic transition zones, which occur in variable geologic and climatic settings and exhibit variable deformational behavior [e.g., *Beaumont et al.*, 2001; *Zeitler et al.*, 2001; *Enkelmann et al.*, 2009; *Koons et al.*, 2013; *Bendick and Ehlers*, 2014]. A key component in the studies of syntaxes is the quantification of spatial and temporal variations in rock exhumation to both decipher the dynamics and relative contributions of different processes (climatic, erosional, and tectonic) to syntaxis formation and evaluate contending exhumation models [e.g., *Zeitler et al.*, 2001; *Enkelmann et al.*, 2009, 2015a; *Koons et al.*, 2010, 2013; *Bendick and Ehlers*, 2014].

One well-established location for studies of syntaxis deformation and exhumation is the glaciated St. Elias syntaxis in southeast Alaska and western Canada (Figure 1) [e.g., *Berger et al.*, 2008; *Enkelmann et al.*, 2009, 2015a; *Spotila and Berger*, 2010; *Chapman et al.*, 2012; *Falkowski et al.*, 2014]. Two different sampling strategies for thermochronology, namely, bedrock and detrital sampling, have previously been used to quantify the exhumation history of the St. Elias Mountains [e.g., *O'Sullivan et al.*, 1997; *Enkelmann et al.*, 2008, 2009, 2015a; *Berger et al.*, 2008; *McAleer et al.*, 2009; *Grabowski et al.*, 2013; *Falkowski et al.*, 2014]. Bedrock data suffer from a biased signal because those samples can only be taken in the foothills or at high-elevation, ice-free ridges, while the youngest rocks that record the most rapid exhumation are expected to occur at low elevations in the glaciated valleys [e.g., *Fitzgerald and Gleadow*, 1990]. Sand-sized detritus from rivers draining the glaciated valleys yields the cooling record from the entire catchment, including those parts above and below the ice [*Enkelmann and Ehlers*, 2015]. This sampling approach revealed the presence of very rapidly exhumed rocks in the syntaxis area through ≤5 Ma old zircon fission track (ZFT) ages [*Enkelmann et al.*, 2009, 2010; *Falkowski et al.*, 2014]. However, the inherent problem of using sand grains for dating is the decrease in spatial

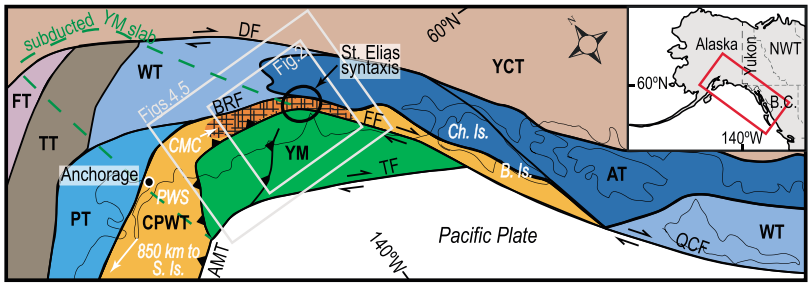

Figure 1. Terrane framework of southeast Alaska and western Canada. DF: Denali Fault, BRF: Border Ranges Fault, QCF: Queen-Charlotte Fault, FF: Fairweather Fault, TF: Transition Fault, AMT: Aleutian Megathrust, YCT: Yukon Composite Terrane, FT: Farewell Terrane, TT: Togiak Terrane, WT: Wrangellia Terrane, PT: Peninsular Terrane, AT: Alexander Terrane, CPWT: Chugach-Prince William Terrane, YM: Yakutat microplate, CMC: Chugach Metamorphic Complex, PWS: Prince William Sound, S. Is.: Sanak Island, Ch. Is.: Chichagof Island, B. Is.: Baranof Island, NWT: Northwest Territories (inset map), B.C.: British Columbia (inset map).

resolution of the cooling signal and provenance. Furthermore, it is difficult to extract fresh minerals from detritus for reliable higher-temperature thermochronometric analyses like $^{40}Ar/^{39}Ar$ dating, which are necessary to constrain timing and depth of rapid exhumation.

In this study, we overcome the previous problems associated with quantifying the spatial and temporal patterns of exhumation by studying cobble-sized detritus from the Seward-Malaspina and Hubbard-Valerie glaciers. These extremely large glaciers cover the main catchments of the St. Elias syntaxis area. Cobbles have the advantage over sand-sized material in that information about individual lithologies in the source region is preserved and that multiple dating techniques on different, unweathered minerals can be applied to the same sample. We present zircon U-Pb ages and lithologic information from thin sections to determine the provenance of 27 cobbles from the two glacial catchments. The cooling history of the rocks was quantified through a large temperature range (500–60°C) using amphibole and biotite $^{40}Ar/^{39}Ar$, apatite fission track (AFT), and apatite and zircon (U-Th)/He (AHe and ZHe, respectively) dating. Additionally, four bedrock samples from the Fairweather Range east of the syntaxial region have been analyzed for biotite $^{40}Ar/^{39}Ar$ cooling ages for comparison of higher-temperature cooling outside the St. Elias syntaxis. To better understand the cooling history of the syntaxis area, the new data are put into a regional geologic context of Cenozoic orogenic evolution by extracting typical cooling histories from published geochronologic and thermochronologic bedrock data from along orogenic strike.

2. Background

The St. Elias Mountains formed due to the ongoing shallow subduction since the late Eocene [*Plafker et al.*, 1994; *Finzel et al.*, 2011] and oblique collision since 15–12 Ma [e.g., *O'Sullivan and Currie*, 1996; *Grabowski et al.*, 2013; *Falkowski et al.*, 2014] of the Yakutat microplate with the North American margin in southeast Alaska (Figure 1). Transform motion along the plate boundary segment represented by the dextral strike-slip Fairweather Fault transitions across the St. Elias syntaxis into flat-slab subduction of the Yakutat slab and deformation of the Cenozoic, western sedimentary cover in the fold-and-thrust belt (Figure 2) [e.g., *Plafker et al.*, 1994; *Bruhn et al.*, 2004, 2012; *Chapman et al.*, 2012]. In the syntaxis area, strain accumulates and rocks exhume rapidly from great depths as indicated by Plio-Pleistocene detrital ZFT cooling ages (inset map in Figure 2) [*Enkelmann et al.*, 2009, 2010; *Falkowski et al.*, 2014]. In contrast, rocks on the southern, coastal flanks of the St. Elias Mountains exhume rapidly but along shallower paths [e.g., *Meigs et al.*, 2008; *Enkelmann et al.*, 2010, 2015b]. High exhumation rates in this convergent setting are assisted by high glacial erosion rates that are estimated to be among the highest in the world with up to 10 mm/yr on time scales of 10^3 to 10^5 years based on sediment accumulation rates offshore [*Hallet et al.*, 1996; *Jaeger et al.*, 1998; *Sheaf et al.*, 2003; *Gulick et al.*, 2015] and ≥2 mm/yr over 10^6 year time scales based on thermochronology [e.g., *McAleer et al.*, 2009; *Spotila and Berger*, 2010; *Grabowski et al.*, 2013]. Glaciation of the St. Elias Mountains began ~5.6 Ma and intensified at the Pliocene/Pleistocene transition [*Lagoe et al.*, 1993].

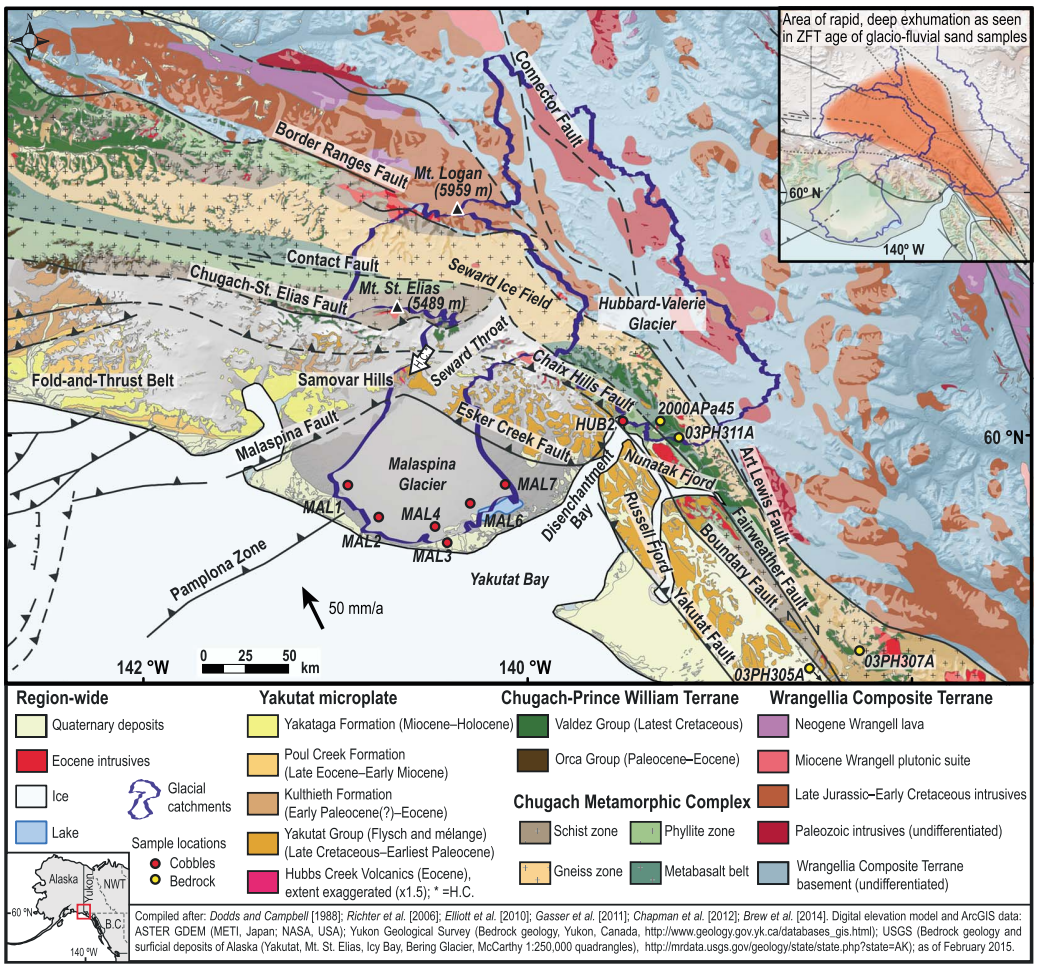

Figure 2. Geologic overview of the St. Elias Mountains including sample locations. For exact sample location of 03PH305A see Figure 4a or Figure S6 in the supporting information. The inset map displays the area of most rapid and deep exhumation in the St. Elias syntaxis and northern Fairweather Fault area based on ≤5 Ma ZFT cooling ages from sand-sized detritus [*Enkelmann et al.*, 2009, 2010; *Falkowski et al.*, 2014].

The Seward-Malaspina (~3900 km^2) and Hubbard-Valerie (~4050 km^2) glacial systems cover the syntaxial region and are surrounded by the highest peaks of the orogen (up to 5959 m at Mount Logan; Figure 2). The Seward Ice Field, with ice thicknesses of >600–800 m [*Rignot et al.*, 2013], drains south through the narrow 4–6 km wide Seward Throat into the 80 km wide Malaspina piedmont glacier (Figure 2), which is up to 600 m thick and extends to 400 m below sea level [*Rignot et al.*, 2013]. The current deformational front of the Cenozoic fold-and-thrust belt runs underneath the western part of the Malaspina lobe with shallow northwest dipping thrusts characterized by frequent, shallow seismic activity [e.g., *Doser and Lomas*, 2000; *Bruhn et al.*, 2004; *Cotton et al.*, 2014]. Northeast dipping thrust and reverse faults within the Yakutat basement bound the Malaspina lobe to the northeast (Figure 2). A partly exposed mountain ridge east of Mount Logan separates the Seward Ice Field in the south from the Hubbard Glacier to the north (Figure 2). The 500–950 m thick ice of the Hubbard Glacier flows for >100 km southeast before it turns south and drains into Disenchantment Bay (Figure 2), making it the largest tidewater glacier in Alaska [*Molnia*, 2008; *Rignot et al.*, 2013]. Close to its terminus, the Hubbard Glacier is joined by the 40 km long Valerie Glacier from the west. The Fairweather Fault runs beneath the Hubbard Glacier snout and along the Valerie Glacier valley (Figure 2).

The geology of the ice-free mountain ridges that surround the Seward-Malaspina and Hubbard-Valerie glaciers is used here to infer the geology in the ice-covered catchments (Figure 2) [e.g., *Hudson et al.*,

1977a, 1977b; *Dodds and Campbell*, 1988; *Plafker et al*., 1989, 1994; *Israel*, 2004; *Pavlis et al*., 2004, 2012; *Richter et al*., 2006; *Chapman et al*., 2012]. Most importantly for this study, previous workers have identified different terranes that underlie the catchments, which are utilized to identify the provenance of the investigated cobbles. Previously accreted terranes of the study area include the Wrangellia Composite Terrane south of the Denali Fault and north of the Border Ranges Fault, the Chugach Terrane south of the Border Ranges Fault and north of the Contact and Fairweather Faults, and the Prince William Terrane south of the Contact Fault and north of the Chugach-St. Elias Fault (Figures 1 and 2). The southern Seward-Malaspina catchment also contains rocks of the currently colliding Yakutat microplate.

In the study area, the Wrangellia Composite Terrane encompasses the Wrangellia and Alexander Terranes, which became juxtaposed in the late Paleozoic and accreted to the North American margin during Middle Jurassic–Late Cretaceous time [e.g., *Jones et al*., 1977; *Gardner et al*., 1988; *Plafker et al*., 1989; *Trop et al*., 2002]. The Wrangellia Composite Terrane is composed of Cambrian–Late Triassic back-arc basin strata, volcanic island arcs, and Upper Triassic greenstone and limestone [e.g., *Hillhouse*, 1977; *Nokleberg et al*., 1994]. Overlying strata include Upper Jurassic–Lower Cretaceous flysch and Paleogene alluvial strata in the Denali Fault area, as well as the Oligocene–Recent Wrangell volcanic belt (Figure 2) [e.g., *Berg et al*., 1972; *Richter et al*., 1990; *Plafker et al*., 1994]. The Wrangellia Composite Terrane is associated with various phases of arc magmatism, abundantly intruded by Upper Jurassic–Cretaceous plutons, and is pervasively metamorphosed [e.g., *Dodds and Campbell*, 1988; *Nokleberg et al*., 1994].

The Chugach and Prince William Terranes represent a Cretaceous–Eocene accretionary complex of deep-water turbidites derived from a Late Cretaceous–Paleocene volcanic arc with Jurassic metaplutonic basement, most likely the Coast Plutonic Complex of today's British Columbia [*Dumoulin*, 1988; *Farmer et al*., 1993; *Garver and Davidson*, 2015]. In the study area, the Chugach Terrane is composed of the Maastrichtian Valdez Group and the Prince William Terrane comprises the Paleocene–lower Eocene Orca Group (Figure 2) [e.g., *Plafker et al*., 1994]. In the St. Elias Mountains, the Chugach and Prince William Terranes are mainly characterized by the ~55–50 Ma, greenschist–amphibolite facies Chugach Metamorphic Complex (Figures 1 and 2), which formed during a spreading ridge subduction event that is associated with the near-trench Sanak-Baranof plutonic belt [e.g., *Sisson and Hollister*, 1988; *Gasser et al*., 2011].

The Yakutat microplate is a 15–30 km thick, northwestward tapering oceanic plateau [*Christeson et al*., 2010; *Worthington et al*., 2012] that is overlain in the east by Campanian–lower Paleocene Yakutat Group flysch and mélange sequences [*Plafker*, 1987], which represent a remnant accretionary complex metamorphosed to zeolite–prehnite-pumpellyite facies [e.g., *Hudson et al*., 1977b; *Dusel-Bacon et al*., 1993; *Worthington et al*., 2012]. In the west, the Yakutat microplate is overlain by $\leq$10 km thick, eastward thinning Cenozoic strata of the Poul Creek, Kulthieth, and Yakataga formations (Figure 2) [*Ferris et al*., 2003; *Eberhart-Phillips et al*., 2006; *Gulick et al*., 2007; *Worthington et al*., 2010]. These strata were sourced from the Coast Plutonic Complex (Poul Creek and Kulthieth formations) and the Chugach and Prince William Terranes (Yakataga Formation) [*Perry et al*., 2009]. Kulthieth and Yakataga formations as well as Yakutat Group rocks are exposed in the Yakutat microplate part of the Seward-Malaspina catchment (Figure 2).

3. Methods

3.1. Samples

This study builds on the analyses of *Grabowski et al*. [2013], who investigated 59 cobbles (10–30 cm size) using petrographic thin sections and ZHe dating to identify the lithologies that were exhumed most rapidly under the Seward-Malaspina Glacier. *Grabowski et al*. [2013] collected samples on top of the debris-covered outer lobe of the Malaspina Glacier as outwash is directly shed into the ocean (Figure 2). Sample selection of a variety of representative lithologies was mainly based on the potential presence of datable mineral phases. The sample set is therefore neither representative of the abundance of rock types (cf. point counting by *Grabowski et al*. [2013]) nor of a quantitative analysis of catchment erosion. In this study, we analyzed a subset of 22 of the cobbles collected by *Grabowski et al*. [2013], which yielded enough datable mineral phases. These cobbles are denoted "MAL" (for Malaspina). Additionally, five cobbles from the sediment fan built up at the western Hubbard Glacier terminus (Figure 2) were collected for this study. Those are denoted "HUB" (for Hubbard). The sediment fan constitutes a mix of sediment from the Hubbard and Valerie glaciers, and therefore, both catchments are considered as the source.

Table 1. Cobble Sample List and Summary of Zircon U-Pb Ages[a]

Sample	Lat (°N) Long (°W)	Lithology	Zircon U-Pb Age (Ma) (2σ)	*N*	Remarks
MAL1-8		Migmatitic gneiss	-	-	No zircons
MAL1-14	59.8592 140.89585	Amphibolite	30.8 ± 0.8	4	Crystallization age
MAL1-19		Aplite	46.4 ± 1.0	6	Crystallization age
MAL2-4	59.77705 140.78952	Granitoid	50.8 ± 1.0	17	Crystallization age
MAL2-10		Paragneiss	335–81/83.8 ± 1.3	19/11	Detrital age range/max. depositional age of sedimentary protolith
MAL2-16		Micaschist	72–49	17	Detrital age range
MAL3-2		Pyroclastic	50–46	8	Detrital age range
MAL3-8	59.70058 140.40393	Orthogneiss	52.3 ± 7.3	2	Lower intercept, protolith age
MAL3-19		Granitoid	277.1 ± 6.7	4	Crystallization age
MAL4-5		Paragneiss	60–48/49.4 ± 0.5	18/6	Detrital age range/max. depositional age of sedimentary protolith
MAL4-6		Igneous mylonite	53.3 ± 0.3	19	Igneous protolith age
MAL4-9	59.74943 140.48363	Orthogneiss	150.0 ± 1.0	29	Protolith age
MAL4-16		Paragneiss	279–56/56.3 ± 0.6/48.7 ± 0.9	16/7/2	Detrital age range/max. depositional age of sedimentary protolith/ metamorphic age
MAL4-21		Metasedimentary mylonite	493–58	21	Detrital age range of sedimentary protolith
MAL6-5		Orthogneiss	151.0 ± 0.7	39	Protolith age
MAL6-23	59.81708 140.30245	Orthogneiss	52.4 ± 0.4	28	Protolith age
MAL6-24		Paragneiss	76–50/52.8 ± 0.5	20/13	Detrital age range/youngest population
MAL7-2		Gabbro	49.4 ± 0.4	10	Crystallization age
MAL7-3		Meta-quartzdiorite	181.6 ± 0.8	29	Protolith age
MAL7-6	59.8669 140.10847	Pyroclastic	50.3 ± 0.3	31	Crystallization age
MAL7-14		Granitoid	50.9 ± 1.4	13	Crystallization age
MAL7-20		Granitoid	48.5 ± 0.6	23	Crystallization age
HUB2-2		Granitoid	-	-	No analysis
HUB2-3		Meta-quartzdiorite	-	-	No analysis
HUB2-5	60.040383 139.54253	Granodiorite	-	-	No analysis
HUB2-7		Hornblende-gabbro	-	-	No analysis
HUB2-8		Mylonite	-	-	No analysis

[a]Unless otherwise noted, the reported zircon U-Pb ages represent concordia ages for (meta-)igneous rocks and age ranges for (meta-)sedimentary rocks, whereas the number of single-grain analyses used to obtain the value(s) is given in the neighboring column (*N*). In addition, the maximum depositional age for sedimentary rocks or protoliths and the age of metamorphism are given when conclusive (notes in the Remarks column). Single-grain analyses as well as concordia diagrams and histograms can be found in the supporting information (Table S2 and Figure S1).

All mineral separates of the 27 cobbles were produced by standard density and magnetic procedures and purified by hand picking. Details of analytical procedures can be found in the supporting information (Text S1).

3.2. Provenance and Cooling Histories

The provenance of 21 Seward-Malaspina cobbles was examined using petrographic analyses of thin sections and zircon U-Pb dating. For one Seward-Malaspina cobble and the five Hubbard cobbles, no crystallization ages are available and the provenance is based on petrographic information and $^{40}Ar/^{39}Ar$ ages. The cooling histories of individual cobbles were reconstructed using multiple thermochronometer analyses with different closure temperatures. These were amphibole and biotite $^{40}Ar/^{39}Ar$ dating with closure temperatures of 500 ± 50°C [*Harrison*, 1982] and 300 ± 50°C [*Harrison et al.*, 1985], respectively, ZHe analyses reflecting a

180 ± 20°C [*Reiners et al.*, 2004] closure temperature, as well as AFT with 110 ± 10°C [*Gleadow and Duddy*, 1981] and AHe dating with 60 ± 15°C [*Farley*, 2000] closure temperatures. In the following, ZFT cooling ages will be discussed together with the cobble cooling ages. The closure temperature for ZFT is 250 ± 40°C but can also be higher for zircons of low radiation damage (young zircons and/or low-uranium zircons) [*Tagami et al.*, 1996; *Brandon et al.*, 1998; *Rahn et al.*, 2004].

4. Results

4.1. Zircon U-Pb Dating

The interpretation of zircon U-Pb ages depends on the sample type analyzed. Generally, zircon U-Pb ages of magmatic rocks refer to the magmatic event and zircon crystallization from the melt, while zircons with metamorphic overgrowth in higher-grade metamorphic rocks yield the age of metamorphism. Furthermore, both magmatic and metamorphic zircons can contain old zircon cores that survived incorporation in melt and metamorphism. In sedimentary rocks, the zircon U-Pb age distribution of the source terrain(s) is reflected in the rock sample. This can also be the case for metasediments, as zircon U-Pb ages do not become completely reset during metamorphism [e.g., *Mezger and Krogstad*, 1997]. A summary of the ages for each sample is presented in Table 1. The details of the single-grain analyses of individual samples as well as concordia diagrams and histograms can be found in the supporting information (Text S1.1, Table S2, and Figure S1). Of the 21 cobbles, eight magmatic cobbles with a range of ages between 277.1 ± 6.7 Ma and 30.8 ± 0.8 Ma (Table 1) were dated. These cobbles show no zircons with inherited older cores (Table S2). Two pyroclastic cobbles yielded ages around 50 Ma, which represent the time of the volcanic eruption(s) (Table 1). As the single-grain ages show a slight spread in both samples, the cobbles probably represent reworked volcanic material from more than one eruption.

The 11 metamorphic cobbles include six metasedimentary and five metaigneous rocks (Table 1). The metasedimentary cobbles have Carboniferous-Eocene age distributions ranging between ~493 Ma and ~48 Ma (concordant ages only) with the vast majority being $<$200 Ma (Table S2). Age distributions of single-grain ages of metasedimentary cobbles reflect the age distribution of their source area, which is discussed later in the text. One of these cobbles (MAL4-16, Table S2) includes a zircon with a metamorphic rim that may reflect ~48 Ma metamorphism causing overgrowth on a ~57 Ma zircon. The metaigneous cobbles yield Early Jurassic–Eocene protolith ages between 181.6 ± 0.8 Ma and 52.3 ± 7.3 Ma (Table 1). Zircons of metaigneous cobbles do not show prominent metamorphic rims, which means that their crystallization age was determined, not the time of the metamorphic event. It is notable that half of the U-Pb ages are ~50 Ma (Table 1).

4.2. $^{40}Ar/^{39}Ar$ Dating

Of eight amphibole samples measured, five yielded meaningful $^{40}Ar/^{39}Ar$ cooling ages that range between 181.0 ± 0.6 Ma and 15.8 ± 0.4 Ma (1σ) (Table 2). The remaining three show (i) an argon profile that is too disturbed for an age estimate (amphibolite MAL1-14), (ii) an argon loss profile suggesting a minimum crystallization age of ~276 Ma and a maximum age of ~139 Ma of thermal resetting (metaquartzdiorite HUB2-3), and (iii) a profile characterized by a combination of argon loss and excess argon (gabbro MAL7-2) (Table 2 and Figures S2l, S2h, and S2n). However, for MAL7-2, the inverse isochron data in combination with the sample's crystallization age of ~49 Ma (Table 1) justifies using an age of 42.0 ± 2.7 Ma (Table 2). For more details concerning the analysis see the supporting information (Text S1.2, Data Set S1, and Figures S2a–S2o).

The seven biotite $^{40}Ar/^{39}Ar$ cooling ages of the cobbles range between 50.4 ± 0.2 Ma and 41.8 ± 0.3 Ma, which are all plateau ages comprising at least 75% of the ^{39}Ar (Table 2). Three of the four bedrock biotite $^{40}Ar/^{39}Ar$ analyses yielded interpretable cooling ages that are presented in Table 3 and in the supporting information (Dataset S1 and Figures S2p–S2s). The ages range between 42.4 ± 1.1 Ma and ~5–3.5 Ma (Table 3). Biotite from tonalite 03PH305A experienced argon loss and does not provide a reliable age. Argon analysis of biotite from the mylonitic tonalite (2000APa45) does not yield a robust cooling age, but suggests cooling through ~300°C between 5 Ma and ~3.5 Ma (Table 3). This sample is from an intrusion of Eocene age located just north of the Fairweather Fault at its northern tip at the Hubbard Glacier terminus (Figure 2). The only other Pliocene $^{40}Ar/^{39}Ar$ cooling age from the region is known from an amphibolite-facies schist ~110 km farther southeast just south of the Fairweather Fault [*Hudson et al.*, 1977b]. The meaning of the age, i.e., whether it represents (localized) contact metamorphism due to an unexposed pluton or exhumational cooling, is not known [*Hudson et al.*, 1977b].

Table 2. Summary of Cobble $^{40}Ar/^{39}Ar$ Ages[a]

Sample	Lithology	Min	Total Gas Age ±1σ (Ma)	WMPA ±1σ (Ma) MSWD, % of ^{39}Ar	IIA ±1σ (Ma) MSWD, $^{40}Ar/^{36}Ar$ Steps Used/Total # Steps
HUB2-2	Granitoid	Bt	49.8 ± 0.3	**50.0 ± 0.3** 0.1, 88.8	50.1 ± 1.0 0.1, 275 ± 110 4–17/17
HUB2-8	Mylonite	Bt	49.7 ± 0.5	**49.8 ± 0.3** 0.01, 89.8	50.0 ± 2.5 0.01, 267 ± 220 4–21/21
MAL2-10	Paragneiss	Bt	50.2 ± 0.2	**50.4 ± 0.2** 0.2, 96.8	50.7 ± 0.6 0.1, 261 ± 58 3–20/20
MAL2-16	Micaschist	Bt	47.9 ± 0.2	**48.0 ± 0.2** 0.2, 96.0	48.0 ± 1.4 0.2, 301 ± 86 4–16/16
MAL3-8	Orthogneiss	Bt	41.4 ± 0.2	**41.8 ± 0.3** 0.1, 74.9	41.5 ± 1.7 0.1, 372 ± 570 7–19/19
MAL6-23	Orthogneiss	Bt	48.4 ± 0.1	**48.7 ± 0.2** 0.2, 93.4	49.5 ± 0.6 0.1, 276 ± 26 4–21/21
MAL6-24	Gneiss	Bt	48.5 ± 0.2	**48.8 ± 0.2** 0.2, 85.2	49.3 ± 0.8 0.2, 274 ± 38 6–20/20
HUB2-3	Meta-quartzdiorite	Am	248.3 ± 0.2	-	276.0 ± 1.8[b] 0.1, 308 ± 14 25–28/28
HUB2-5	Granodiorite	Am	148.7 ± 0.2	151.5 ± 0.6 0.5, 26.6	**151.2 ± 1.1** 0.1, 311 ± 15 20–25/25
HUB2-7	Hornblende-Gabbro	Am	24.3 ± 0.5	**25.5 ± 0.4** 0.2, 99.8	26.1 ± 0.6 2.8, 296 ± 2 1–19/19
MAL1-8	Migmatitic gneiss	Am	16.3 ± 0.5	**15.8 ± 0.4** 0.5, 100	15.8 ± 0.8 0.5, 306 ± 8 1–21/21
MAL1-14	Amphibolite	Am	602.0 ± 1.4	-	-[c]
MAL6-23	Orthogneiss	Am	50.9 ± 0.1	**51.2 ± 0.2** 0.3, 97.7	51.4 ± 0.5 0.3, 290 ± 12 7–25/25
MAL7-2	Gabbro	Am	62.4 ± 0.2	-	42.0 ± 2.7 1.4, 409 ± 10 13–19/20
MAL7-3	Meta-quartzdiorite	Am	175.2 ± 0.2	**181.0 ± 0.6** 1.0, 90.2	180.6 ± 1.4 1.8, 311 ± 21 10–23/24

[a]Min: Mineral; WMPA: Weighted mean plateau age; MSWD: Mean square weighted deviation; IIA: Inverse isochron age; Bt: Biotite; Am: Amphibole.
[b]Argon loss-profile with ~276 Ma as minimum crystallization age and ~139 Ma as maximum age of thermal resetting.
[c]Disturbed profile, no age estimate possible. Ages in bold font are used in the interpretation. Details can be found in the supporting information (Text S1.2, Figures S2a–S2o, and Data Set S1).

4.3. Zircon and Apatite (U-Th)/He Dating

The new ZHe ages from the HUB cobbles are presented in Table 4. Three of the HUB cobbles yield reproducible ages of 34.84 ± 3.0 Ma (HUB2-2), 5.79 ± 1.33 Ma (HUB2-5), and 4.82 ± 0.02 Ma (HUB2-8). For HUB2-3 single-grain ages are 10.34 Ma and 24.18 Ma (Table 4). Because the younger of the single-grain ages is younger than the AFT age of that sample (17.2 ± 1.4 Ma; Table 5), the true ZHe age is suggested to be closer to the older of the two zircon aliquots, i.e., 24 Ma.

ZHe ages of the Seward-Malaspina cobbles were published by *Grabowski et al.* [2013]. They measured 59 Seward-Malaspina cobbles and obtained five distinct ZHe age populations: ~2.7 Ma, ~12 Ma, ~27 Ma,

Table 3. Summary of Bedrock Cooling Ages[a]

Sample	T_c (°C) Lat (°N) Long (°W) Elevation (m)	60 ± 15 Apatite (U-Th)/He ±1σ (Ma)	180 ± 20 Zircon (U-Th)/He ±1σ (Ma)	250 ± 40 Zircon Fission Track ±1σ (Ma)	300 ± 50 Biotite $^{40}Ar/^{39}Ar$ ±1σ (Ma)	Lithology, Terrane
2000APa45	60.03214 139.328241 309	-	-	-	~5–3.5	Mylonitic tonalite CT
03PH305A	59.1281 138.089 88	1.82 ± 0.5[b] *N* = 31	2.45 ± 0.17[b] *N* = 2	27.5 ± 1.5[b] *N* = 15	-	Tonalite YM
03PH307A	59.4378 138.2429 243	2.34 ± 0.33[b] N = 16	13 ± 0.8[b] N = 2	16.5 ± 0.8[b] N = 15	42.4 ± 1.1	Granodiorite CT
03PH311A	60.0225 139.2058 1610	0.89 ± 0.11[b] *N* = 22	1.96 ± 0.09[b] *N* = 2	4.5 ± 0.3[b] *N* = 15	35.3 ± 0.5	Granite CT

[a]Closure temperature (T_c) of the thermochronometric systems after *Harrison et al.* [1985], *Brandon et al.* [1998], *Farley* [2000], and *Reiners et al.* [2004].
[b]Ages from *McAleer et al.* [2009], who used multiple multialiquot AHe analysis; *N*: Number of grains analyzed, CT: Chugach Terrane, YM: Yakutat microplate. For 03PH305A no reliable age estimate is possible due to argon loss. For details of $^{40}Ar/^{39}Ar$ analyses see Data Set S1 and Figures S2p–S2s in the supporting information.

~36 Ma, and ~53 Ma. The youngest four of the age populations are represented in the subset of cobbles used here (Table 6). Those have been interpreted as being associated with subduction and collision processes of the Yakutat microplate with the North American Plate since the late Eocene [*Grabowski et al.*, 2013]. The new HUB cobble ZHe ages fall into the same age range (Table 6).

Table 4. Zircon and Apatite (U-Th)/He Data for Single-Aliquot Analyses of Cobbles[a]

Sample_ Aliquot #	Min	^{4}He (mol)	^{238}U (mol)	^{235}U (mol)	^{232}Th (mol)	^{147}Sm (mol)	α-Uncorrected Age (Ma)	Ft	α-Corrected Age (Ma)	Mean Age ±1SD (Ma)
HUB2-2_1	Zr	2.01E−14	5.34E−13	3.92E−15	1.66E−13	na	27.17	0.73	36.96	
HUB2-2_2	Zr	2.91E−14	8.52E−13	6.26E−15	2.11E−13	na	24.99	0.76	32.72	34.84 ± 3.0
HUB2-3_1	Zr	4.37E−14	3.86E−12	2.84E−14	1.71E−12	na	7.94	0.77	10.34	
HUB2-3_2	Zr	1.63E−13	5.80E−12	4.26E−14	4.29E−12	na	18.52	0.77	24.18	17.26 ± 9.78
HUB2-5_1	Zr	1.04E−13	1.83E−11	1.35E−13	5.05E−12	na	4.14	0.85	4.85	
HUB2-5_2	Zr	8.69E−14	1.07E−11	7.83E−14	4.72E−12	na	5.72	0.85	6.73	5.79 ± 1.33
HUB2-8_1	Zr	1.85E−14	3.49E−12	2.56E−14	1.40E−12	na	3.76	0.78	4.81	
HUB2-8_2	Zr	2.09E−14	4.08E−12	3.00E−14	1.23E−12	na	3.71	0.77	4.83	4.82 ± 0.02
MAL1-8_1	Ap	-	-	-	-	-	-	-	-	
MAL1-8_2	Ap	2.28E−17	1.09E−14	8.03E−17	0.00E+00	3.29E−15	1.61	0.76	2.13	
MAL1-8_3	Ap	6.28E−18	4.48E−15	3.29E−17	0.00E+00	3.71E−15	1.08	0.70	1.54	1.84 ± 0.41
MAL2-10_1	Ap	6.85E−15	1.15E−12	8.47E−15	0.00E+00	9.64E−13	4.58	0.78	5.90	
MAL2-10_2	Ap	1.19E−14	1.71E−12	1.26E−14	3.21E−14	1.11E−12	5.35	0.75	7.13	6.52 ± 0.87
MAL2-10_3	Ap	9.60E−15	5.39E−14	3.96E−16	0.00E+00	3.30E−14	135.78	0.75	~~181.02~~	
MAL2-16_1	Ap	1.19E−15	2.94E−13	2.16E−15	2.34E−14	4.01E−13	3.06	0.77	3.99	
MAL2-16_2	Ap	7.59E−16	1.95E−13	1.43E−15	1.84E−14	3.65E−13	2.92	0.71	4.09	
MAL2-16_3	Ap	2.82E−15	6.31E−13	4.63E−15	3.78E−14	6.94E−13	3.39	0.75	4.54	4.20 ± 0.29
MAL3-8_1	Ap	7.78E−17	1.42E−13	1.04E−15	1.18E−14	1.23E−13	0.41	0.63	0.66	
MAL3-8_2	Ap	1.16E−16	1.32E−13	9.68E−16	1.48E−14	1.19E−13	0.66	0.63	1.05	
MAL3-8_3	Ap	4.94E−17	7.26E−14	5.33E−16	3.80E−14	7.70E−14	0.47	0.59	0.79	0.83 ± 0.20
MAL6-23_1	Ap	1.23E−14	2.79E−12	2.05E−14	1.34E−12	5.96E−13	3.07	0.77	4.00	
MAL6-23_2	Ap	1.13E−14	2.73E−12	2.01E−14	1.55E−12	5.49E−13	2.83	0.79	3.58	
MAL6-23_3	Ap	1.33E−14	3.83E−12	2.81E−14	1.51E−12	7.16E−13	2.47	0.75	3.29	3.62 ± 0.35
MAL7-3_1	Ap	3.74E−16	5.17E−13	3.80E−15	6.17E−13	6.23E−14	0.44	0.67	0.66	
MAL7-3_2	Ap	4.80E−16	2.80E−13	2.06E−15	3.29E−13	8.38E−14	1.04	0.68	~~1.54~~	
MAL7-3_3	Ap	3.47E−16	4.89E−13	3.59E−15	5.17E−13	7.75E−14	0.44	0.71	0.62	0.64 ± 0.03

[a]Min: Mineral, Zr: Zircon, Ap: Apatite, na: not applicable, Ft: α-ejection correction factor [*Farley et al.*, 1996], SD: Standard deviation. MAL2-10_3 and MAL7-3_2 were rejected as outliers.

Table 5. Summary of Apatite Fission Track Data[a]

Sample	N	N_s	N_i	ρ_s (cm^{-2})	ρ_i (cm^{-2})	ρ_d (cm^{-2})	χ^2 (%)	AFT Age ±1σ (Ma)
HUB2-2	10	4	63	8.83E+03	1.06E+05	5.12E+05	14.75	3.8 ± 2.0
HUB2-3	25	206	715	1.55E+05	5.05E+05	5.07E+05	5.97	17.2 ± 1.4
HUB2-5	27	40	608	2.97E+04	3.98E+05	5.02E+05	0.006	4.8 ± 1.3
HUB2-7	8	3	108	6.67E+03	1.89E+05	4.96E+05	43.14	1.6 ± 1.0

[a]AFT ages calculated using the external detector method and a ζ factor of 237 ± 5 cm^2 yr (E.E.) for dosimeter glass IRMM540; for $\chi^2 > 5\%$ the pooled age is reported, for $\chi^2 < 5\%$ the mean age is reported; N: number of grains dated, N_s, N_i: number of spontaneous and induced tracks, respectively; ρ_s, ρ_i: spontaneous and induced track densities, respectively, ρ_d: induced track density in external detector over dosimeter glass.

Table 6. Summary of Cooling Ages and Zircon U-Pb Ages of MAL and HUB Cobbles[a]

	Cooling Ages				Provenance Tools	
T_c (°C)	60 ± 15 *110 ± 10*	180 ± 20	300 ± 50	500 ± 50		
Sample	Apatite (U-Th)/He ±1SD (Ma), *Fission track* ± 1σ (Ma)	Zircon (U-Th)/He ±1SD (Ma)	Biotite ^{40}Ar/^{39}Ar ± 1σ (Ma)	Amphibole ^{40}Ar/^{39}Ar ± 1σ (Ma)	Zircon U-Pb ± 2σ (Ma)	Cobble Lithology
			Wrangellia Composite Terrane Provenance			
MAL7-3	0.64 ± 0.03	3.0 ± 0.2	-	181.0 ± 0.6	181.6 ± 0.8	Meta-quartzdiorite; Qtz, Fsp, Hbl; Qtz and Fsp strongly altered, Hbl with cracks and inclusions
HUB2-3	*17.2 ± 1.4*	~24–17	-	276.0 ± 1.8[b]	-	Meta-quartzdiorite; strongly altered, Ser in Fsp; Chl, Bt in Am; greenschist facies, retrograde alteration
HUB2-5	*4.8 ± 1.3*	5.79 ± 1.3	-	151.2 ± 1.1	-	Granodiorite; Qtz, Fsp, Am
MAL3-19	-	11.0 ± 1.9	-	-	277.1 ± 6.7	Granitoid; Bt, Pl, Hbl, Opx, Cpx, Op
MAL4-9	-	32.3 ± 10.1	-	-	150.0 ± 1.0	Orthogneiss; Kfs, Grt, Bt, Qtz
MAL6-5	-	36.9 ± 9.9	-	-	151.0 ± 0.7	Orthogneiss; Qtz, Bt, Chl, Ms, Fsp
			Chugach and Prince William Terranes Provenance			
MAL7-14	-	2.4 ± 0.2	-	-	50.9 ± 1.4	Granitoid; Fsp, Bt, Qtz, Ms, Chl
MAL7-20	-	2.5 ± 0.3	-	-	48.5 ± 0.6	Granitoid; Pl, Hbl, Opx, Cpx, Ap
MAL3-8	0.83 ± 0.2	2.6 ± 0.3	41.8 ± 0.3	-	52.3 ± 7.3	Orthogneiss; Qtz, Bt, Fsp, Px, some Ms, Ep
MAL2-4	-	13.3 ± 1.6	-	-	50.8 ± 1.0	Granitoid (Qtz-diorite?); Qtz, Fsp to Ser, Px
MAL6-24	-	14.5 ± 0.8	48.8 ± 0.2	-	76–50	Paragneiss; Bt, Fsp, Qtz, Ep
MAL2-16	4.2 ± 0.29	15.5 ± 0.7	48.0 ± 0.2	-	72–49	Micaschist; Bt, Chl, Fsp with Ep and Ser, Grt, Qtz
MAL6-23	3.6 ± 0.35	15.5 ± 1.5	48.7 ± 0.2	51.2 ± 0.2	52.4 ± 0.4	Orthogneiss; Bt, Qtz, Fsp, Cpx, some Ms
MAL4-5	-	16.4 ± 1.3	-	-	60–48	Paragneiss; Pl, Qtz, Bt, small Ms, small Grt
MAL2-10	6.5 ± 0.87	16.7 ± 5.6	50.4 ± 0.2	-	335–81	Paragneiss; Bt, Qtz, Pl, Ms, Grt
MAL4-16	-	16.8 ± 2.6	-	-	279–56	Paragneiss; Qtz, Fsp, Bt, Chl
MAL4-6	-	29.2 ± 1.4	-	-	53.3 ± 0.3	Igneous mylonite; Fsp, Qtz, Bt
HUB2-2	*3.8 ± 2.0*	34.8 ± 3.0	50.0 ± 0.3	-	-	Granitoid; FSp, Qtz, Bt, Chl, Op (Py?)
HUB2-8	-	4.8 ± 0.02	49.8 ± 0.3	-	-	Mylonite; Qtz, Fsp, Bt, Am; few Am altered
			Yakutat Microplate Provenance			
MAL3-2	-	6.2 ± 1	-	-	50–46	Pyroclastic
MAL7-6	-	8.4 ± 1.9	-	-	50.3 ± 0.3	Pyroclastic
			Uncertain Provenance			
MAL1-14	-	2.2 ± 0.3	-	-	30.8 ± 0.8	Amphibolite; Act, Pl
MAL1-19	-	2.3 ± 0.4	-	-	46.4 ± 1.0	Aplite; Fsp, Qtz, Grt
MAL1-8	1.84 ± 0.41	2.4 ± 0.5	-	15.8 ± 0.4	-	Fine-grained, strongly deformed migmatitic gneiss; Am, Fsp, Ep; Ep developing in foliation, Am a little altered
MAL7-2	-	3.2 ± 1.03	-	42.0 ± 2.7	49.4 ± 0.4	Gabbro; 80% Pl, light green Am, Cpx in Am strongly altered, low metamorphic grade
MAL4-21	-	20.5 ± 1.3	-	-	493–58	Metasedimentary mylonite; Bt, Grt, Ep, Ms, Qtz, Kfs
HUB2-7	*1.6 ± 1.0*	-	-	25.5 ± 0.4	-	Hornblende-gabbro; Hbl, Pl, Qtz; medium-grained

[a]Closure temperature (T_c) of the thermochronometric systems after *Gleadow and Duddy* [1981], *Harrison* [1982], *Harrison et al.* [1985], *Farley* [2000], and *Reiners et al.* [2004]. ZHe data of MAL cobbles from *Grabowski et al.* [2013]. SD: Standard deviation. Mineral abbreviations following *Kretz* [1983].
[b]Minimum crystallization age.

AHe ages of six MAL cobbles range between 6.52 ± 0.87 Ma and 0.64 ± 0.03 Ma (Table 4). This result is consistent with other published AHe ages from the wider St. Elias syntaxis area and has been interpreted in terms of high precipitation and glacial erosion rates as well as Quaternary fault activity [e.g., *Spotila and Berger*, 2010; *Enkelmann et al*., 2015b].

4.4. Apatite Fission Track Dating

Three AFT ages are reported as pooled ages because they passed the χ^2 test (i.e., $\chi^2 > 5\%$); they are 17.2 ± 1.4 Ma, 3.8 ± 2 Ma, and 1.6 ± 1.0 Ma (1σ; Table 5). HUB2-5 is reported as a mean age (4.8 ± 1.3 Ma, 1σ; Table 5) as it failed the χ^2 test (i.e., $\chi^2 < 5\%$), which indicates a larger scatter between single-grain ages. Reset sedimentary bedrock samples or igneous bedrock samples, as in this case, should generally pass the test, demonstrating that individual grains belong to the same cooling age population [*Galbraith*, 1981]. However, if track counts are small, as in the case of HUB2-5, where eight of 27 grains yielded zero spontaneous track counts and the remaining grains do not exceed seven spontaneous track counts, the χ^2 probability is not a reliable statistic [e.g., *Galbraith*, 2005].

5. Discussion

5.1. Cobble Provenance

Here we discuss the cobble provenance and their cooling histories with respect to their sources. Table 6 summarizes available crystallization and cooling ages and is sorted by cobble provenance.

5.1.1. Wrangellia Composite Terrane and Chugach-Prince William Terrane Provenance

Early Cretaceous and older U-Pb and $^{40}Ar/^{39}Ar$ cooling ages are typical for rocks of the Wrangellia Composite Terrane [e.g., *Dodds and Campbell*, 1988; *Plafker et al*., 1994; *O'Sullivan and Currie*, 1996; *Enkelmann et al*., 2010]. For example, widespread Upper Jurassic plutonic rocks have been mapped at the southern margin of the Wrangellia Composite Terrane including the northern part of the Seward-Malaspina catchment and most of the Hubbard catchment [e.g., *Armstrong*, 1988; *Dodds and Campbell*, 1988; *Israel*, 2004]. The Wrangellia Composite Terrane provenance of Early Cretaceous and older cobbles becomes even more evident considering that the crystallization ages of the remaining cobbles are ~50 Ma (Table 6). Those ~50 Ma ages are characteristic of the early Eocene metamorphism and magmatism in the Chugach and Prince William Terranes. The $^{40}Ar/^{39}Ar$ cooling ages of both biotite and amphibole from cobbles with ~50 Ma U-Pb ages are just a few million years younger (~1–10 Myr) and thus indicate rapid initial cooling that is consistent with the current understanding of the cooling history of the Chugach Metamorphic Complex (Figures 1 and 2) [e.g., *Sisson et al*., 2003; *Gasser et al*., 2011].

Six metasedimentary cobbles yield detrital U-Pb age distributions, but the number of single-grain analyses per sample ($N = 16–21$; Table 1) is not high enough to quantitatively compare them to previously published detrital zircon age distributions of the studied terranes [e.g., *Gehrels et al*., 2009; *Amato and Pavlis*, 2010; *Kochelek et al*., 2011; *Rick et al*., 2014]. Qualitatively, the range of the youngest zircons (55–49 Ma; Table S2) of micaschist MAL2-16, and paragneisses MAL4-16 and MAL4-5, is typical of the Orca Group of the Prince William Terrane [e.g., *Davidson et al*., 2011]. The occurrence of micaschist is also typical for the Prince William Terrane (Figure 2). Conversely, the age range and distribution of paragneiss MAL2-10 (335–81 Ma) resembles that of the Valdez Group of the Chugach Terrane [e.g., *Rick et al*., 2014]. The provenance of the metasedimentary mylonite MAL4-21 (Table 1) is not easily assignable and discussed in section 5.1.3.

5.1.2. Yakutat Microplate Provenance

The pyroclastic cobbles assigned to the Yakutat microplate (MAL3-2 and MAL7-6; Table 6) yield crystallization ages indistinguishable from the ~50 Ma ages that we argued to represent the Chugach Metamorphic Complex. However, their lithology is distinctly different. The cobbles are reworked pyroclastic material from early Eocene volcanic eruptions. The sediments must have been reheated, probably by burial, to have their ZHe ages reset at temperatures ≥180°C, followed by exhumation around 8–6 Ma (Table 6). In the study area, such a scenario is only known for the Yakutat microplate. The only lower Eocene volcanics are the Hubbs Creek Volcanics of the Samovar Hills (white arrow in Figure 2) (T. L. Pavlis, personal communication, 2015). *Plafker* [1987] described the sequence as hundreds of meters of basalt, agglomerate, and tuff that overlie, possibly conformably, rocks of the Yakutat Group. Whole-rock K-Ar minimum crystallization ages and biostratigraphy of the overlying unit indicate an age of 50 ± 3.9 Ma [*Plafker*, 1987]. Thus, the age of the Hubbs Creek Volcanics corresponds to the zircon U-Pb ages of the pyroclastic cobbles. Resetting of the ZHe system through reheating may have occurred with burial by Eocene–Holocene sediments. However, mid-Eocene

to upper Miocene–lower Pliocene strata are missing due to an erosional event sometime between the early Miocene and the latest Miocene–earliest Pliocene [*Chapman et al*., 2012]. If those sediments were thick enough (at least 6–7 km with an assumed paleogeothermal gradient of 25–30°C/km), then the scenario fits the crystallization age and latest Miocene exhumation of the two cobbles (Table 6).

5.1.3. Cobbles of Uncertain Provenance

The provenance of six cobbles is unclear, because their crystallization and cooling ages are either not known from the study area (MAL1-8, MAL1-14, MAL1-19, MAL7-2, and HUB2-7; Table 6), or not distinct (MAL4-21; Table 6). The metasedimentary mylonite MAL4-21 yields a U-Pb single-grain age distribution of 493–58 Ma, with most ages 190–80 Ma (Tables 1 and S2). The range and distribution resembles neither the Valdez nor Orca Group, and no $^{40}Ar/^{39}Ar$ cooling ages are available (Table 6). The overall age distribution and the range of youngest zircons in sample MAL4-21 are similar to the mélange of the McHugh Complex, the northernmost and oldest belt of the Chugach accretionary complex that has been mapped in Prince William Sound and a potential equivalent on Baranof Island (Figure 1) [*Haeussler et al*., 2005; *Amato and Pavlis*, 2010] but is not known from the study area. The U-Pb single-grain age distribution is also similar to the distribution of the Yakutat Group exposed in the Seward-Malaspina catchment [*Enkelmann et al*., 2009]. Thus, this cobble could be either from the Border Ranges suture zone in the oldest, northernmost belt of the Chugach Terrane, if it occurs continuously along the entire terrane, or from the Yakutat Group close to the Yakutat-Chugach suture zone (Fairweather-Contact Fault connection; Figure 2). Both faults have been active at different times during the Cenozoic [e.g., *Roeske et al*., 2003; *Bruhn et al*., 2004].

Three cobbles of uncertain provenance have younger than Eocene zircon U-Pb crystallization or amphibole $^{40}Ar/^{39}Ar$ cooling ages. The amphibolite MAL1-14 yields a U-Pb age of 30.8 ± 0.8 Ma, and the migmatitic gneiss MAL1-8 and the gabbro HUB2-7 have amphibole $^{40}Ar/^{39}Ar$ cooling ages of 15.8 ± 0.4 Ma and 25.5 ± 0.4 Ma, respectively (Table 6). Only a few ages have been reported that are that young: conventional K-Ar ages and $^{40}Ar/^{39}Ar$ ages ~23–15 Ma from the Fairweather Range, particularly from the Chugach Terrane in the Nunatak Fjord and Hubbard terminus areas (Figure 2) [e.g., *Hudson et al*., 1977a, 1977b; *Loney and Himmelberg*, 1983; *Smart et al*., 1996; *Sisson et al*., 2003; *Gasser et al*., 2011]. *Gasser et al*. [2011] interpreted the $^{40}Ar/^{39}Ar$ cooling ages of the Nunatak area as a slower cooling of the Chugach Metamorphic Complex than in its western and central parts west of the syntaxis due to differences in convergent components at the plate margin. *Sisson et al*. [2003] associated an early Miocene amphibole $^{40}Ar/^{39}Ar$ cooling age with an eastward tilting of the area east of the Fairweather Fault and then a later, Neogene cooling due to uplift and exhumation in response to deformation in the Fairweather fault zone.

An alternative to explaining the $^{40}Ar/^{39}Ar$ cooling age of gabbro HUB2-7 with exhumational cooling at the plate boundary is thermal relaxation after Oligocene intrusion, which might also be reflected by the 30.8 ± 0.8 Ma U-Pb age of amphibolite MAL1-14 (Table 6). Mafic intrusions are not mapped within the study area but are known from a narrow mafic-ultramafic belt farther southeast in the Fairweather Range and as far south as Chichagof and Baranof islands (Figure 1). These intrusions have been interpreted as being associated with transpression at the Fairweather Fault [e.g., *Rossman*, 1963; *Plafker and MacKevett*, 1969; *Loney et al*., 1975; *Loney and Himmelberg*, 1983; *Brew et al*., 2014]. As the St. Elias syntaxis area is extensively ice covered, hitherto undetected Oligocene mafic intrusions may occur in the Hubbard and Seward Glacier region as well, due to either in-place intrusion or lateral displacement along the Fairweather Fault. The only known occurrence of a possibly Oligocene gabbro is at Mount Newton, just east of Mount St. Elias (Figure 2) [*Hudson et al*., 1977b; *Dodds and Campbell*, 1988].

In summary, a Chugach Terrane origin of the uncertain cobbles is most likely, a Yakutat microplate origin is possible, and a Wrangellia Composite Terrane origin is unlikely.

5.2. New Cooling Histories From the St. Elias Syntaxis

The time-temperature plots of Figure 3 show the new cooling ages from the Seward-Malaspina and Hubbard-Valerie cobbles and the three bedrock samples from the Fairweather Range. By combining similar cooling paths of different samples, five dominant paths can be distinguished (1–5 in Figures 3b and 3c). Cooling path 1 comprises the majority of cobbles with Chugach and Prince William provenance and is characterized by rapid early Eocene cooling to ~300°C after early Eocene crystallization and metamorphism in the Chugach Metamorphic Complex (Figure 3b).

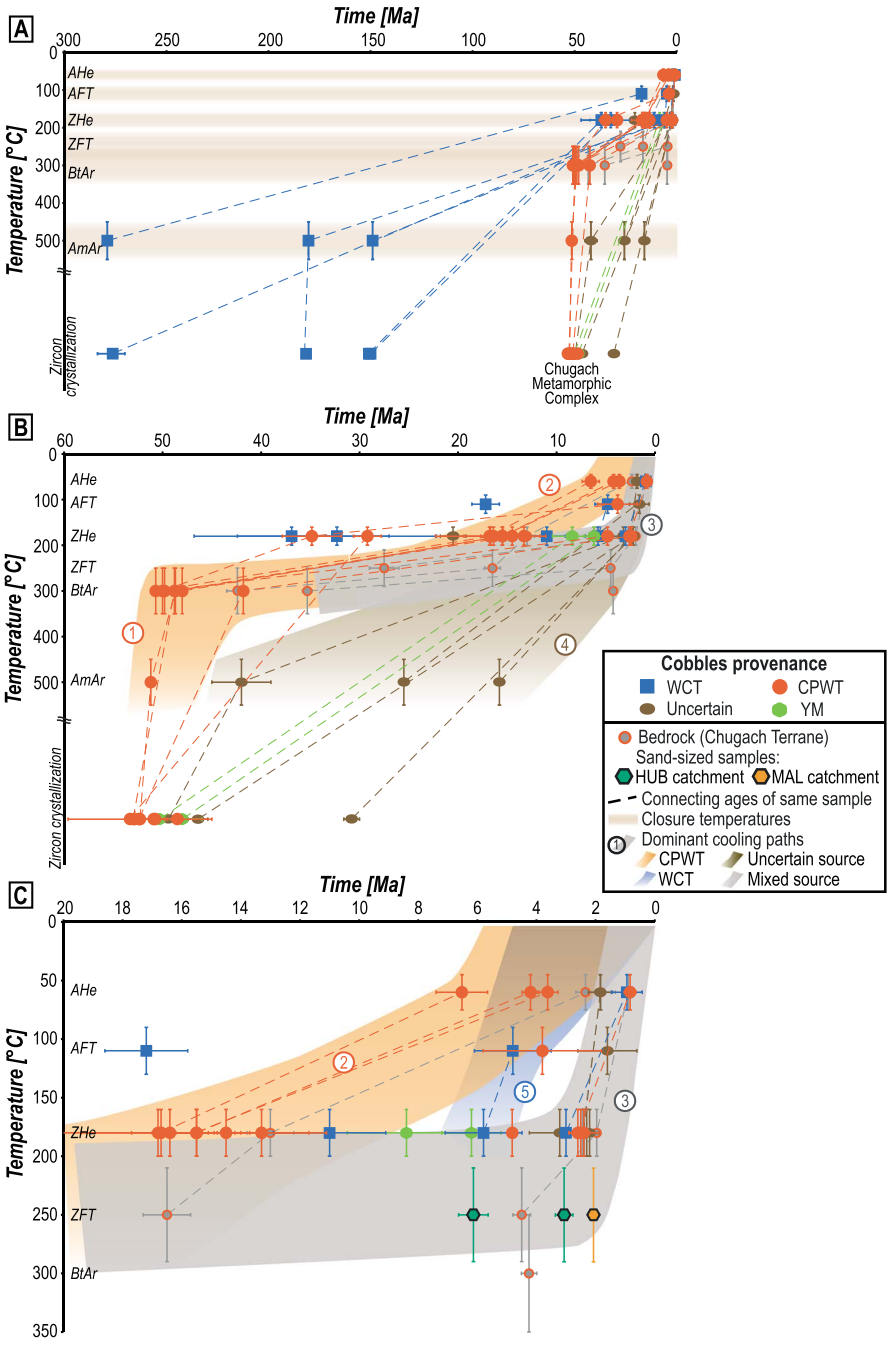

Figure 3. (a)Time-temperature plot of all new cooling ages of this study and previous thermochronometric ages of the three bedrock samples with new $^{40}Ar/^{39}Ar$ ages, (b) zoomed into 60–0 Ma, and (c) 20–0 Ma/< 350°C. Cooling ages are plotted against their corresponding closure temperatures, AHe: apatite (U-Th)/He, AFT: apatite fission track, ZHe: zircon (U-Th)/He, ZFT: zircon fission track, BtAr: biotite $^{40}Ar/^{39}Ar$, AmAr: amphibole $^{40}Ar/^{39}Ar$. Dominant cooling paths are marked in colored bands and numbered in (b) and (c). The colors of the cooling paths relate to the provenance of the samples describing the path. CPWT: Chugach and Prince William Terranes, WCT: Wrangellia Composite Terrane. The youngest ZFT cooling age populations of sand samples from the MAL and HUB catchments are given for comparison (c).

Cooling path 2 combines Chugach and Prince William Terrane cobbles exhibiting renewed acceleration of cooling to ZHe closure in the Miocene. Further cooling to AHe closure and surface temperature occurred in late Miocene–Pleistocene time (Figure 3C), which is interpreted as exhumational cooling in the absence of heat sources in the study region at that time [e.g., *Plafker et al*., 1994]. Cooling path 3 includes cobbles and a bedrock sample (03PH311A) of the Chugach and Prince William Terrane that did not cool to ZHe closure in the Miocene, like those of path 2, but during a rapid cooling phase in the Plio-Pleistocene (Figures 3b and 3c). Path 3 also includes rocks of the Wrangellia Composite Terrane and of uncertain source (Chugach Terrane or Yakutat microplate, cf. section 5.1.3), which cooled rapidly through ZFT to AHe closure temperatures in the St. Elias syntaxis area (Figure 3c). Cooling path 3 may describe the same path as previously dated detrital sand samples from the syntaxis that suggested a focused area of rapid and deep exhumation (inset map in Figure 2) [*Enkelmann et al*., 2009; *Falkowski et al*., 2014]. The youngest ZFT age population from three Seward-Malaspina sand samples is 2.1 ± 0.1 Ma comprising 30% of the dated grains ($N = 312$; yellow polygon symbol in Figure 3c), and the youngest two ZFT age populations from a Hubbard-Valerie sand sample are 6.1 ± 0.5 Ma and 3.1 ± 0.3 Ma comprising 46% and 39% of the grains, respectively ($N = 105$; dark green polygon symbols in Figure 3c). The fact that cobbles from different terranes exhibit this cooling pattern supports the conclusion by *Grabowski et al*. [2013], who suggested, based on the lithology of the cobbles with young ZHe ages, that a large areal extent of rapid exhumation exists in the Seward-Malaspina catchment and beyond.

Cooling path 4 combines the cobbles of uncertain provenance that yielded younger than early Eocene crystallization or amphibole $^{40}Ar/^{39}Ar$ cooling ages (Figure 3). Eocene to Miocene cooling is poorly confined and different for all cobbles in this group, but for the lower-temperature cooling, this path follows the Plio-Pleistocene part of path 3 with the exception of MAL4-21, which has a ZHe age of ~21 Ma (Figure 3b). Cooling path 5 highlights the rapid cooling from ZHe to AFT closure of Wrangellia Composite Terrane cobble HUB2-5 at ~5 Ma, similar to the cooling observed at Mount Logan [*O'Sullivan and Currie*, 1996]. The HUB2-5 cobble is a granodiorite with an ~150 Ma amphibole $^{40}Ar/^{39}Ar$ cooling age and could be derived from the Late Jurassic Mount Logan Batholith [*Dodds and Campbell*, 1988; *O'Sullivan and Currie*, 1996]. This comparison and the designation of an individual path for a single sample become clearer in the regional synthesis that includes cooling paths from Mount Logan (sections 5.3.2 and 5.3.3).

5.3. Regional Cooling Histories

A discussion of the St. Elias syntaxis cooling history in a regional context requires division of the St. Elias Mountains into four areas along orogenic strike (Area 1–4; Figure 4a). For each area, time-temperature plots were created and the dominant cooling paths were identified (Figures 4b–4e). Note that in the plots, bedrock and cobble cooling ages are plotted together and, with the exception of the Mount Logan profile (Area 2; Figures 4a and 4c), elevation differences are not marked.

5.3.1. Area 1

Area 1 is located west of the syntaxial region and contains only data from the Chugach and Prince William Terranes to avoid the coastal, thermochronologically mostly unreset fold-and-thrust belt [e.g., *Meigs et al*., 2008; *Enkelmann et al*., 2010] and the Oligocene–Recent Wrangell volcanic belt to the north (Figure 4a) [*Richter et al*., 1990]. Cooling of this area is characterized by early Eocene–Oligocene post-magmatic and post-metamorphic cooling of the Chugach Metamorphic Complex (path 1) and post-Oligocene cooling due to erosion and exhumation of path 2 (Figure 4b). This latter cooling was probably in response to flat-slab subduction of the Yakutat microplate [e.g., *Perry et al*., 2009; *Enkelmann et al*., 2010]. Additionally, Oligocene–Miocene cooling of rocks from ZFT to AHe closure occurred (path 2? in Figure 4b), which might represent a wider range of cooling path 2 than in the cobble data (Figures 3b and 3c) with a younging of AHe ages from west to east and with increasing elevation toward the St. Elias syntaxis (>2000 m). The wide age range in the AHe ages in the western area can be explained by the high sensitivity of these low-temperature thermochronometric systems to changes in erosion and topography [e.g., *Ehlers and Farley*, 2003].

5.3.2. Area 2

Area 2 comprises the Seward Ice Field region (Figure 4a) and includes the MAL cobbles (Figure 4c). The main cooling paths 1–4 of the new cobble data are supported by the few bedrock samples from this area. Important information on the cooling history come from the ~4000 m elevation profile at Mount Logan [*O'Sullivan and Currie*, 1996; *Enkelmann et al*., 2010; *Spotila and Berger*, 2010]. Paths L1, L2, and L3 represent the upper, middle, and lower elevation parts of the exposed Mount Logan profile, respectively (Figure 4c). As

expected, samples from the lower part of the profile reveal younger cooling ages than samples collected at higher elevations. The two Wrangellia Composite Terrane cobbles that lie within uncertainty in path L1 or L2 (MAL4-9 and MAL6-5; Figure 4c) and the Chugach Prince William cobble MAL4-6 with a ~29 Ma ZHe cooling age (Figure 3b) are thus very likely derived from Mount Logan from >3000 m. The Wrangellia Composite Terrane cobbles are likely sourced from the Jurassic Mount Logan Batholith and the Chugach Terrane cobble from the Eocene King Peak Pluton of Mount Logan. Mount Logan cooling paths L1 and L2 are distinct from other post-early Eocene cooling paths (Figure 4c) as these rocks were collected at higher elevations than other bedrock samples. The cobble samples complement the profile for lower, ice-covered elevations (<1780 m) and show path 3 cooling with rapid Plio-Pleistocene exhumational cooling (Figure 4c).

5.3.3. Area 3

The Hubbard-Valerie catchment and immediate surroundings constitute Area 3, which includes the HUB cobbles and is mainly composed of Wrangellia Composite Terrane rocks (Figures 4a and 4d). Therefore, many Paleozoic–Mesozoic ages of the higher-temperature $^{40}Ar/^{39}Ar$ systems are present (see Figure S8 for >60 Ma cooling ages) and the Chugach Metamorphic Complex cooling of path 1 is only roughly defined by a few samples from the southern part of Area 3 (Figure 4d). Cooling path 2 is not discernible here, but paths 3 and 4 are. Path 3 is only seen in Chugach Terrane samples in this area, but a few relatively young, Neogene Wrangellia Composite Terrane bedrock AHe cooling ages from elevations >2000 m are available from the northern syntaxis area that fit into cooling path 5 (Figures 3 and 4d).

5.3.4. Area 4

Area 4 is the northern part of the Fairweather fault zone east of the Hubbard Glacier terminus. Area 4 is underlain by rocks of Wrangellia Composite and Chugach Terranes and Yakutat microplate (Figures 4a and 4e), which explains the complexity of cooling histories compared to western areas. Paths 1, 3, and 4 occur here, but additional paths 6 and 7 are defined by Chugach Terrane and Yakutat microplate samples, respectively (Figure 4e). Even though cooling path 1 of the Chugach Metamorphic Complex occurs here like in the areas to the west, path 6 represents a deviation from that with later (around 35 Ma) but equally rapid cooling. Other samples of the Chugach Terrane/Chugach Metamorphic Complex cooled at a slower rate and were contained in path 4, including the only sample for which a crystallization age is available in this area [*Gasser et al*., 2011]. All of these samples are close to the Fairweather Fault and mostly from the Nunatak Fjord area (Figures 4a and S6). This pattern is interpreted as reflecting transpressional deformation at the plate boundary, especially within the zone of strain accumulation at the northern tip of the Fairweather Fault, where it begins to bend (Figure 4a). The mylonitic tonalite 2000APa45 (Table 3) and schist 68Apr57F [*Hudson et al*., 1977b] of Pliocene biotite $^{40}Ar/^{39}Ar$ ages are both located close to the mapped trace of the Fairweather Fault (Figures 4a, 4e, and S6) and indicate significant shear deformation in the Pliocene, when rapid exhumation began in the syntaxis and northern Fairweather Fault areas.

5.4. Summary of Cooling Histories of the St. Elias Mountains

Figure 5 summarizes the spatiotemporally nonuniform cooling histories along the Cenozoic Alaskan margin. A simplified interpretation of the cooling paths 1–7, as extracted from Figures 3 and 4b–4e, is given in Figure 5 as well. Additionally, Figure 6 displays the main tectonic and geologic events of the study area in relation to the time-temperature paths explained in Figure 5.

The compilation of thermochronometric data reveals the magmatic, metamorphic, and exhumational cooling of the St. Elias Mountains due to Mesozoic–Cenozoic accretion, subduction, and collision at the North American margin. Paleozoic–Mesozoic cooling is mostly recorded in the Wrangellia Composite Terrane north of the Border Ranges Fault, which acted as backstop to Cenozoic accretion and collision of the Yakutat microplate and may not have experienced much erosion and exhumation since [e.g., *Roeske et al*., 2003; *Enkelmann et al*., 2008, 2010]. However, samples from the northern St. Elias Mountains are sparse and cooling ages are mainly from biotite and hornblende K-Ar systems [*Dodds and Campbell*, 1988]. From available data, the Wrangellia Composite Terrane exhibits only in the syntaxis area younger, Neogene and Quaternary cooling due to exhumation (path 5; Figures 3 and 4) [*O'Sullivan and Currie*, 1996; *Enkelmann et al*., 2010; *Spotila and Berger*, 2010; *Grabowski et al*., 2013; *Falkowski et al*., 2014].

The Eocene cooling history of the margin is characterized by near-trench plutonism, and the formation and rapid cooling of the Chugach Metamorphic Complex (path 1; Figures 3 and 4) at rates of ~30–180°C/Myr in an overall compressional tectonic setting [*Gasser et al*., 2011, 2012]. The influence of the subsequently formed

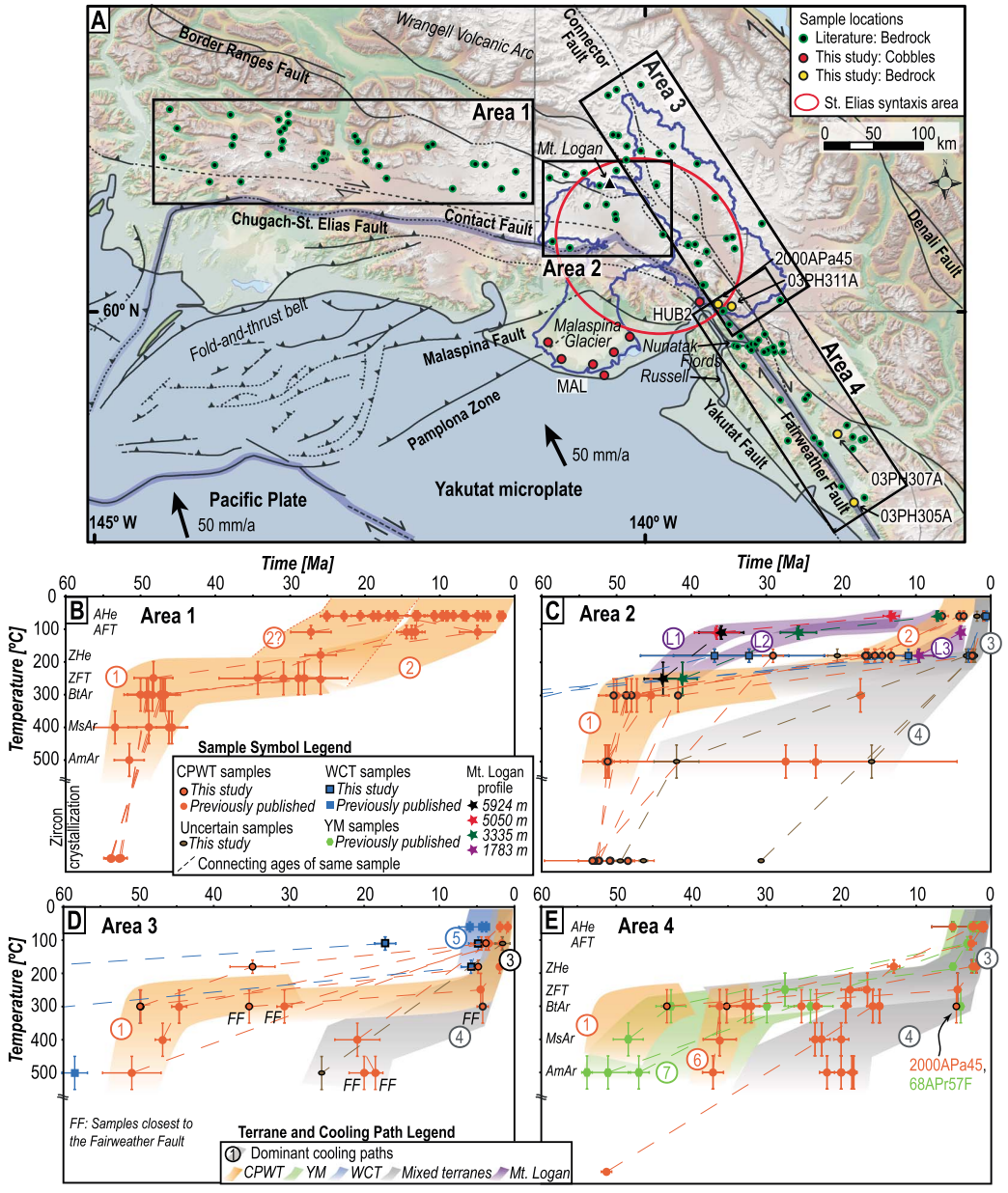

Figure 4. (a) Digital elevation model (ASTER GDEM, 30 m; NASA, METI) of the St. Elias Mountains and Fairweather Range showing (b–e) Areas 1–4 for which time-temperature plots were reconstructed from previously published bedrock and new cobble and bedrock geochronologic and thermochronologic data. Closure temperatures are marked in Figures 4b and 4e using the same abbreviations as in Figure 3, additional: MsAr for muscovite $^{40}Ar/^{39}Ar$. CPWT: Chugach and Prince William Terranes, WCT: Wrangellia Composite Terrane, YM: Yakutat microplate. Data from *Hudson et al.* [1977a, 1977b], *Hudson et al.* [1979], *Dodds and Campbell* [1988], *O'Sullivan and Currie* [1996], *O'Sullivan et al.* [1997], *Sisson et al.* [2003], *Spotila et al.* [2004], *Berger and Spotila* [2008], *Berger et al.* [2008], *Meigs et al.* [2008], *McAleer et al.* [2009], *Enkelmann et al.* [2010, 2015b], *Spotila and Berger* [2010], *Gasser et al.* [2011], and this study. Plate motion vectors from *Plattner et al.* [2007] and *Elliott et al.* [2010]; faults from Yukon Geological Survey (Figure 4a). Sample details can be found in the supporting information (Figures S3–S6 and Data Set S2). In Areas 2–4, >60 Ma cooling ages occur. These are presented in the supporting information (Figures S7–S9).

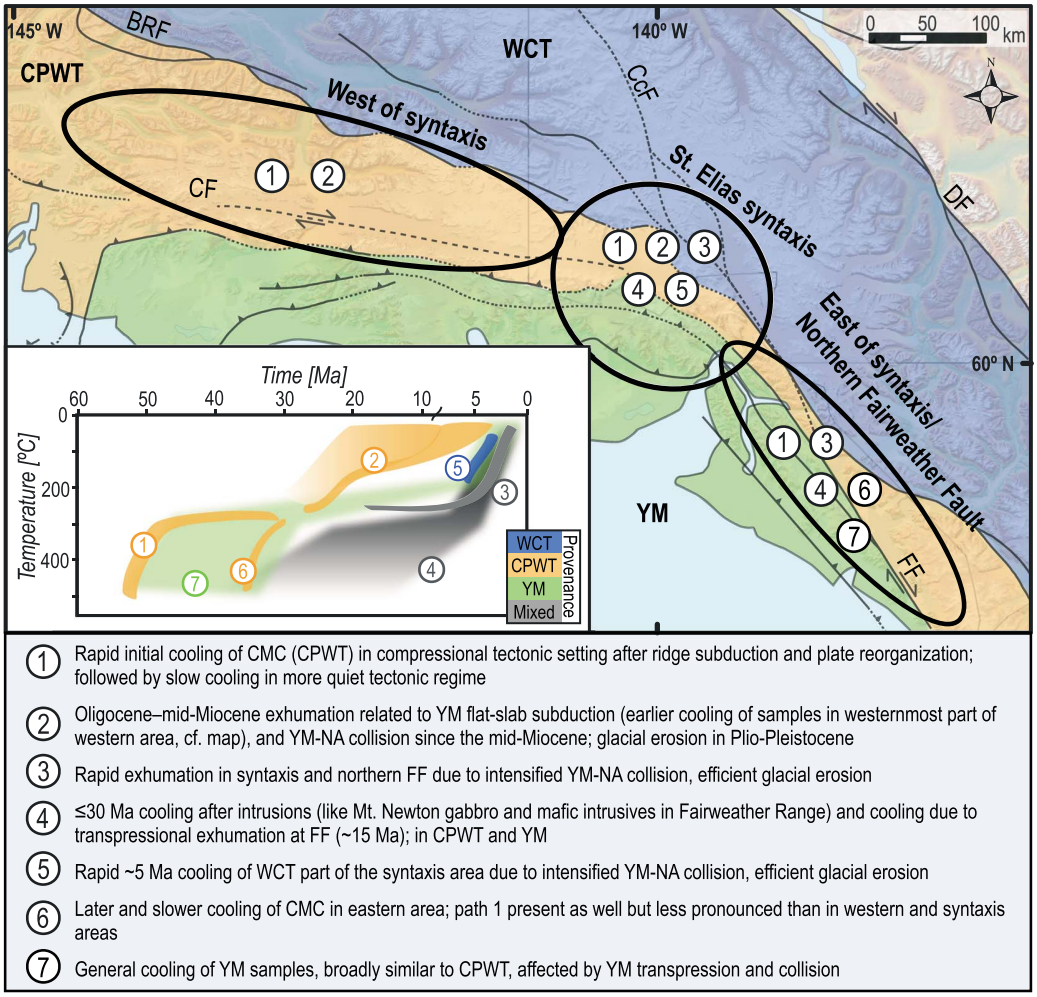

Figure 5. Summary of dominant cooling paths of Areas 1–4, reduced to three areas at the St. Elias syntaxis (Areas 2 and 3; Figure 4a), and areas west (Area 1; Figure 4a) and east (Area 2; Figure 4a) of the syntaxis. The northern part of Area 3 (Figure 4a) mainly contains >60 Ma cooling ages and is not included here. The colors and numbers of cooling paths in the time-temperature plot correspond to cooling path numbers and colors in Figures 3 and 4b–4e and in the map of this figure. Cooling paths are explained at the bottom. BRF: Border Ranges Fault, CcF: Connector Fault, DF Denali Fault, CF: Contact Fault, FF: Fairweather Fault, WCT: Wrangellia Composite Terrane, CPWT: Chugach and Prince William Terranes, YM: Yakutat microplate, NA: North American Plate, CMC: Chugach Metamorphic Complex.

transpressional plate boundary in the eastern area becomes evident through the more variable post-Eocene cooling (paths 1, 4, 6, and 7; Figures 3 and 4). Significant transpressional deformation at the plate boundary since the Oligocene is indicated by exhumational cooling (paths 6, 7, and partly 4; Figures 3 and 4) [e.g., *Sisson et al.*, 2003; *Gasser et al.*, 2011; *McAleer et al.*, 2009; *Falkowski et al.*, 2014] and by transpression-related mafic intrusions and subsequent thermal relaxation (path 4; Figures 3 and 4) [e.g., *Rossman*, 1963; *Plafker and MacKevett*, 1969; *Loney and Himmelberg*, 1983]. Path 4 in the Fairweather Range and St. Elias syntaxis is relatively poorly confined in its >200°C part due to highly variable cooling over short horizontal distances. Thermal overprinting and partial thermal overprinting of country rocks by Eocene–Miocene mafic intrusions (Figure 6) contributed to the variable cooling history of the eastern part of the orogen.

The effects of flat-slab subduction of the Yakutat microplate since the late Eocene/Oligocene include uplift, erosion, and exhumation of the upper plate as reflected in paths 2 and 6 in the syntaxis and western area (Figures 3 and 4) [e.g., *Enkelmann et al.*, 2008; *Perry et al.*, 2009]. Path 2 might also represent the mid-Miocene onset of collision between the Yakutat and North American plates (Figure 6), similar to signals observed in thermochronology of detrital sand samples and bedrock samples from Mount Logan (Figures 3 and 6).

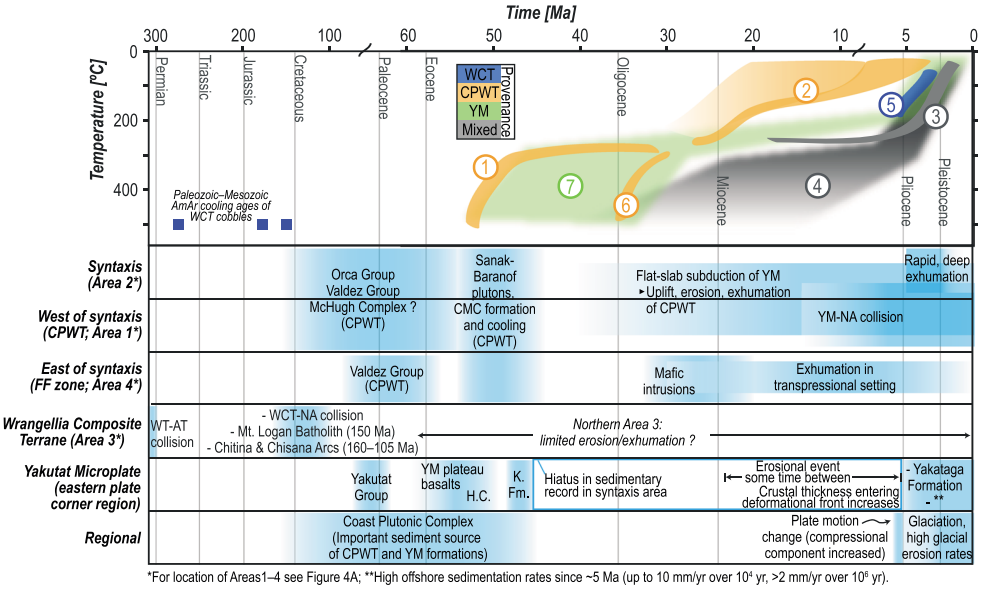

Figure 6. Overview of cooling histories (as in Figure 3) of the St. Elias Mountains and Fairweather Range and tectonic and geologic events divided by area. Note the breaks in the time axis after 100 Ma and 10 Ma. WCT: Wrangellia Composite Terrane, CPWT: Chugach and Prince William Terranes, YM: Yakutat microplate, AmAr: amphibole $^{40}Ar/^{39}Ar$, CMC: Chugach Metamorphic Complex, NA: North American Plate, FF: Fairweather Fault, WT: Wrangellia Terrane, AT: Alexander Terrane, H.C.: Hubbs Creek Volcanics, K. Fm.: Kulthieth Formation. After *Hudson et al.* [1977a, 1977b], *Loney and Himmelberg* [1983], *Engebretson et al.* [1985], *Davis and Plafker* [1986], *Plafker* [1987], *Dodds and Campbell* [1988], *Dumoulin* [1988], *Farmer et al.* [1993], *Lagoe et al.* [1993], *Plafker et al.* [1994], *Pavlis and Sisson* [1995], *Hallet et al.* [1996], *Lagoe and Zellers* [1996], *O'Sullivan and Currie* [1996], *Sheaf et al.* [2003], *Enkelmann et al.* [2008, 2009, 2010, 2015b], *Gehrels et al.* [2009], *McAleer et al.* [2009], *Perry et al.* [2009], *Amato and Pavlis* [2010], *Finzel et al.* [2011], *Gasser et al.* [2011], *Chapman et al.* [2012], *Worthington et al.* [2012], *Grabowski et al.* [2013], *Falkowski et al.* [2014], and this study.

Paths 3 and 5 reflect the localized, rapid Pliocene exhumation of the St. Elias syntaxis and northern Fairweather Fault areas due to the ongoing indentation of the eastern Yakutat plate corner (Figures 3 and 4). Cooling path 3 is revealed by cobble samples and supported by some bedrock samples of different terranes (Figures 4b–4e). Processes that may have influenced deformation at the end of the Miocene include (i) lateral thickening of the Yakutat microplate crust (>25 km) that enters the deformational front [*Christeson et al.*, 2010; *Worthington et al.*, 2012], (ii) an increase in the compressional component of plate collision [*Engebretson et al.*, 1985], and (iii) the beginning of glaciation [e.g., *Lagoe et al.*, 1993] (Figure 6). The localization of strain in the syntaxis area and the glaciation that intensified ~2.6 Ma with Northern Hemisphere cooling led to efficient glacial erosion of highly stressed, easily erodible rocks in valleys [*Lagoe et al.*, 1993; *White et al.*, 1997; *Grabowski et al.*, 2013; *Headley et al.*, 2013].

5.5. Implications for the Evolution of Syntaxis Exhumation

The provenance information and cooling histories obtained from cobbles help to decipher the development of exhumation in the St. Elias syntaxis, where relatively few samples have been dated so far. Prior to this study, the most important data from the syntaxis were the Mount Logan bedrock profile and detrital sand samples from the Malaspina Glacier [*O'Sullivan and Currie*, 1996; *Enkelmann et al.*, 2009]. We have shown here that cobbles complement very well the bedrock and sand samples and also yield additional information. Cooling paths from cobbles show that the onset of rapid exhumation was ~5 Ma. Moreover, complete cooling histories from the syntaxis area were derived for the first time and can be compared to the cooling and exhumation record from other parts of the orogen. This comparison shows similarities and also distinct differences that emphasize the transitional position of the St. Elias syntaxis between the transpressive setting of the Fairweather plate boundary to the east and the compressional and subduction setting to the west (Figure 5).

The St. Elias syntaxis and the northern Fairweather fault zone, especially in the Nunatak Fjord area, have previously been established as rapidly exhuming by thermochronometric, structural, petrographic, and geophysical data, which is supported here [e.g., *Hudson et al*., 1977b; *O'Sullivan et al*., 1997; *Sisson et al*., 2003; *Enkelmann et al*., 2009; *McAleer et al*., 2009; *Gasser et al*., 2011; *Grabowski et al*., 2013; *Falkowski et al*., 2014; *Marechal et al*., 2015]. For the first time, the higher-temperature cooling history of rocks sourced from the most rapidly and deeply exhuming area under the ice of the Seward-Malaspina and Hubbard-Valerie glaciers is presented. This sets important brackets on the maximum amount and duration of rapid rock exhumation, which allows comparing the St. Elias syntaxis with other orogens. The St. Elias syntaxis has been compared with the eastern Himalayan syntaxis, where rocks of lower plate affinity and intrusions from lower crustal depth are exposed and where <2 Ma biotite $^{40}Ar/^{39}Ar$ ages and ZFT ages are observed [*Zeitler et al*., 1989, 2001, 2014; *Enkelmann et al*., 2011]. The higher-temperature $^{40}Ar/^{39}Ar$ systems of the cobbles in the St. Elias Mountains are generally much older (~15–180 Myr; Table 6), and rocks at the high mountain peaks reveal Eocene AFT and ZFT cooling ages [*O'Sullivan and Currie*, 1996], indicating a relatively short duration of rapid exhumation in the syntaxis area. Exhumation rates of 3 mm/yr or higher could not have been sustained for more than a few million years without exposing young $^{40}Ar/^{39}Ar$ ages and removing the entire uppermost crustal layer with the older cooling record.

The amount of exhumation can be estimated from the closure temperature isotherms of the young (<5 Ma) ZFT and old (>15 Ma) biotite $^{40}Ar/^{39}Ar$ systems (~250–300°C versus 300 ± 50°C). Hence, rocks exhumed rapidly from depths corresponding to ~300°C. Using a geothermal gradient of 20–30°C/km suggests a maximum exhumation magnitude of 10–15 km since 5 Ma and most likely less if heat advection is taken into account [e.g., *Reiners and Brandon*, 2006]. This maximum estimate is up to 25–30 km less than the observed exhumation at the eastern Himalayan syntaxis but occurred probably over a shorter time period than at the Himalayan syntaxis, where up to 40 km of exhumation occurred over 3–10 Myr [*Booth et al*., 2009]. Based on a recent synthesis of thermochronometric, geophysical, and geological data, *Enkelmann et al*. [2015a] suggested that the high exhumation rates that developed beginning ~5 Ma at the St. Elias syntaxis have decreased after ~2 Ma. Furthermore, they suggested that the focus of most rapid exhumation shifted southward to its current location on the deforming Yakutat microplate in the Malaspina Glacier and Disenchantment Bay area (Figure 2). Such a short duration of rapid exhumation (2–3 Myr) is in agreement with the calculated limit of the amount of exhumation from the higher temperature $^{40}Ar/^{39}Ar$ data.

The only relatively young biotite $^{40}Ar/^{39}Ar$ cooling age (~5–3.5 Ma; Table 6) from the syntaxis area is from a mylonitic tonalite (2000APa45; Table 3), which is not representative of the rapidly exhuming area but directly of deformation along the Fairweather Fault. This sample may indicate intensified Yakutat-North American collision around 5 Ma in the syntaxial region and significant shear on the Fairweather transform fault that resulted in mylonitization and biotite growth or thermal resetting.

5.6. Applicability of Cobble-Sized Detrital Thermochronology

The geochronology and thermochronology applied on cobbles combine the advantages of bedrock and detrital sampling strategies. Detrital sampling allows investigating the bedrock that is otherwise inaccessible for sampling (e.g., underneath glaciers), but the analysis of sand-sized detritus requires a single-grain analysis and mineral phases that are resistant to weathering such as zircon, apatite, and muscovite. Cobbles can be analyzed like bedrock allowing us to date mineral phases that weather easily (e.g., biotite, hornblende, and potassium feldspar) and use multigrain analysis as well as multiple-aliquot analysis that result in high-precision ages. The question of cobble provenance can be addressed by combining the information of cobble lithology, U-Pb dating of zircons from the cobble, and the entire cooling history. A disadvantage of the cobble technique is that it is costly and time-consuming, and thus not efficient for a high number of cobbles that is required for a statistical analysis of erosion and sediment source in a catchment. Therefore, a combination of analysis of sand- and cobble-sized material appears to be most favorable.

6. Conclusions

In this study, we demonstrate the applicability of cobble-sized detrital thermochronology for exhumation and provenance studies in partly inaccessible catchments. For the St. Elias Mountains, detrital material is invaluable for obtaining an exhumation signal from the lower elevations of ice-filled valleys. The synthesis

of geochronologic and thermochronologic data obtained from the different sampling approaches yields a comprehensive perspective on the cooling and exhumation history of the St. Elias orogen and particularly the ongoing indentation of the Yakutat plate corner into the North American margin. An onset of rapid exhumation at the syntaxis and northern side of the northern Fairweather Fault at ~5 Ma is supported by the cooling histories of cobbles from the Seward-Malaspina and Hubbard-Valerie catchments. The higher-temperature systems reveal that the amount of exhumation since ~5 Ma must have been limited to depths of ~10 km or depths corresponding to ~300°C, which further supports the interpretation of a southward shift in the location of focused, rapid exhumation from the North American Plate to the Yakutat microplate. The geochronometric and thermochronometric data presented here provide a baseline data set that can be used in future geodynamic models, which need spatial and temporal constraints on sediment source and exhumation.

Acknowledgments

All analytical data as well as supporting figures are available in the supporting information. This study was funded by the Deutsche Forschungsgemeinschaft (DFG grants EN-941/1 and EN-941/1-2 to E. Enkelmann) and European Research Council (ERC Consolidator grant 615703 to T. Ehlers). We are very grateful to Terry L. Pavlis for discussions on samples with uncertain provenance and for providing sample 2000APa45, as well as to John I. Garver for discussions about detrital U-Pb age distributions. We also would like to thank Craig Dietsch for looking at some of the thin sections, and Kenneth D. Ridgway for information about the Hubbs Creek Volcanics. Samples 03PH305, 03PH307, and 03PH311 were collected by Peter Haeussler. Special thanks to Blanka Sperner and Anja Obst for supporting the $^{40}Ar/^{39}Ar$ analyses in Freiberg, and to Bruce Idleman and Peter K. Zeitler for help with the $^{40}Ar/^{39}Ar$ measurements at Lehigh University. We appreciate very much the help of Ronny Schönberg and Elmar Reitter during setup of the new analytical procedures of U, Th, and Sm measurements of apatites and zircons at the University of Tübingen. Hartmut Schulz is thanked for help with the scanning electron microscope in Tübingen. The comments and suggestions from Emily Finzel, one anonymous reviewer, and the Associate Editor were very constructive and helped to improve the manuscript significantly.

References

Amato, J. M., and T. L. Pavlis (2010), Detrital zircon ages from the Chugach Terrane, southern Alaska, reveal multiple episodes of accretion and erosion in a subduction complex, *Geology*, *38*, 459–462, doi:10.1130/G30719.1.

Armstrong, R. L. (1988), Mesozoic and Early Cenozoic magmatic evolution of the Canadian Cordillera, *Geol. Soc. Am. Spec. Pap.*, *218*, 55–92, doi:10.1130/SPE218-p55.

Beaumont, C., R. A. Jamieson, M. H. Nguyen, and B. Lee (2001), Himalayan tectonics explained by extrusion of a low-viscosity crustal channel coupled to focused surface denudation, *Nature*, *414*, 738–742, doi:10.1038/414738a.

Bendick, R., and T. A. Ehlers (2014), Extreme localized exhumation at syntaxes initiated by subduction geometry, *Geophys. Res. Lett.*, *41*, 5861–5867, doi:10.1002/2014GL061026.

Berg, H. C., D. L. Jones, and D. H. Richter (1972), Gravina-Nutzotin Belt: Tectonic significance of an upper Mesozoic sedimentary and volcanic sequence in southern and southeastern Alaska, *U.S. Geol. Surv. Prof. Pap.*, *800D*, D1–D24.

Berger, A. L., and J. A. Spotila (2008), Denudation and deformation in a glaciated orogenic wedge: The St. Elias orogen, Alaska, *Geology*, *36*, 523–526, doi:10.1130/G24883A.1.

Berger, A. L., J. A. Spotila, J. B. Chapman, T. L. Pavlis, E. Enkelmann, N. A. Ruppert, and J. T. Buscher (2008), Architecture, kinematics, and exhumation of a convergent orogenic wedge: A thermochronological investigation of tectonic-climatic interactions within the central St. Elias orogen, Alaska, *Earth Planet. Sci. Lett.*, *270*, 13–24, doi:10.1016/j.epsl.2008.02.034.

Booth, A. L., C. P. Chamberlain, W. S. Kidd, and P. K. Zeitler (2009), Constraints on the metamorphic evolution of the eastern Himalayan syntaxis from geochronologic and petrologic studies of Namche Barwa, *Geol. Soc. Am. Bull.*, *121*, 385–407, doi:10.1130/B26041.1.

Brandon, M. T., M. K. Roden-Tice, and J. I. Garver (1998), Late Cenozoic exhumation of the Cascadia accretionary wedge in the Olympic Mountains, northwest Washington State, *Geol. Soc. Am. Bull.*, *110*, 985–1009, doi:10.1130/0016-7606(1998)110<0985:LCEOTC>2.3.CO;2.

Brew, D. A., K. E. Tellier, M. A. Lanphere, D. C. Nielsen, J. G. Smith, and R. A. Sonnevil (2014), Geochronology of plutonic rocks and their tectonic terranes in Glacier Bay National Park and Reserve, southeast Alaska, *U.S. Geol. Surv. Prof. Pap.*, *1776–E*, doi:10.3133/pp1776E.

Bruhn, R. L., T. L. Pavlis, G. Plafker, and L. Serpa (2004), Deformation during terrane accretion in the Saint Elias orogen, Alaska, *Geol. Soc. Am. Bull.*, *116*, 771–787, doi:10.1130/B25182.1.

Bruhn, R. L., J. Sauber, M. M. Cotton, T. L. Pavlis, E. Burgess, N. A. Ruppert, and R. R. Forster (2012), Plate margin deformation and active tectonics along the northern edge of the Yakutat Terrane in the Saint Elias orogen, Alaska, and Yukon, Canada, *Geosphere*, *8*, 1384–1407, doi:10.1130/GES00807.1.

Chapman, J. B., T. L. Pavlis, R. L. Bruhn, L. L. Worthington, S. P. Gulick, and A. L. Berger (2012), Structural relationships in the eastern syntaxis of the St. Elias orogen, Alaska, *Geosphere*, *8*, 105–126, doi:10.1130/GES00677.

Christeson, G. L., S. P. Gulick, H. J. Van Avendonk, L. L. Worthington, R. S. Reece, and T. L. Pavlis (2010), The Yakutat Terrane: Dramatic change in crustal thickness across the Transition Fault, Alaska, *Geology*, *38*, 895–898, doi:10.1130/G31170.1.

Cotton, M. M., R. L. Bruhn, J. Sauber, E. Burgess, and R. R. Forster (2014), Ice surface morphology and flow on Malaspina Glacier, Alaska: Implications for regional tectonics in the St. Elias orogen, *Tectonics*, *33*, 581–595, doi:10.1002/2013TC003381.

Davidson, C., J. I. Garver, H. L. Hilbert-Wolf, and B. Carlson (2011), Maximum depositional age of the Paleocene to Eocene Orca flysch, Prince William Sound, Alaska, paper presented at GSA Annual Meeting Minneapolis.

Davis, A. S., and G. Plafker (1986), Eocene basalts from the Yakutat Terrane: Evidence for the origin of an accreting terrane in southern Alaska, *Geology*, *14*, 963–966, doi:10.1130/0091-7613(1986)14<963:EBFTYT>2.0.CO;2.

Dodds, C. J., and P. B. Campbell (1988), Potassium-argon ages of mainly intrusive rocks in the Saint Elias Mountains, Yukon and British Columbia, *Geol. Surv. Canada paper 87-16*.

Doser, D. I., and R. Lomas (2000), The transition from strike-slip to oblique subduction in southeastern Alaska from seismological studies, *Tectonophysics*, *316*, 45–65, doi:10.1016/S0040-1951(99)00254-1.

Dumoulin, J. A. (1988), Sandstone petrographic evidence and the Chugach-Prince William terrane boundary in southern Alaska, *Geology*, *16*, 456–460, doi:10.1130/0091-7613(1988)016<0456:SPEATC>2.3.CO;2.

Dusel-Bacon, C., B. Csejtey, H. L. Foster, E. O. Doyle, W. J. Nokleberg, and G. Plafker (1993), Distribution, facies, ages, and proposed tectonic associations of regionally metamorphosed rocks in east- and south-central Alaska, *U.S. Geol. Surv. Prof. Pap.*, *1497-C*.

Eberhart-Phillips, D., D. H. Christensen, T. M. Brocher, R. Hansen, N. A. Ruppert, P. J. Haeussler, and G. A. Abers (2006), Imaging the transition from Aleutian subduction to Yakutat collision in central Alaska, with local earthquakes and active source data, *J. Geophys. Res.*, *111*, B11303, doi:10.1029/2005JB004240.

Ehlers, T. A., and K. A. Farley (2003), Apatite (U-Th)/He thermochronometry: Methods and applications to problems in tectonic and surface processes, *Earth Planet. Sci. Lett.*, *206*, 1–14, doi:10.1016/S0012-821X(02)01069-5.

Elliott, J. L., C. F. Larsen, J. T. Freymueller, and R. J. Motyka (2010), Tectonic block motion and glacial isostatic adjustment in southeast Alaska and adjacent Canada constrained by GPS measurements, *J. Geophys. Res.*, *115*, B09407, doi:10.1029/2009JB007139.

Engebretson, D. C., A. Cox, and R. G. Gordon (1985), Relative motions between oceanic and continental plates in the Pacific basin, *Geol. Soc. Am. Spec. Pap.*, *206*, 1–60, doi:10.1130/SPE206-p1.

Enkelmann, E., and T. A. Ehlers (2015), Evaluation of detrital thermochronology for quantification of glacial catchment denudation and sediment mixing, *Chem. Geol.*, *411*, 299–309, doi:10.1016/j.chemgeo.2015.07.018.
Enkelmann, E., J. I. Garver, and T. L. Pavlis (2008), Rapid exhumation of ice-covered rocks of the Chugach-St. Elias orogen, SE-Alaska, *Geology*, *36*, 915–918, doi:10.1130/G2252A.1.
Enkelmann, E., P. K. Zeitler, T. L. Pavlis, J. I. Garver, and K. D. Ridgway (2009), Intense localized rock uplift and erosion in the St. Elias orogen of Alaska, *Nat. Geosci.*, *2*, 360–363, doi:10.1038/NGEO502.
Enkelmann, E., P. K. Zeitler, J. I. Garver, T. L. Pavlis, and B. P. Hooks (2010), The thermochronological record of tectonic and surface process interaction at the Yakutat–North American collision zone in southeast Alaska, *Am. J. Sci.*, *310*, 231–260, doi:10.2475/04.2010.01.
Enkelmann, E., T. A. Ehlers, P. K. Zeitler, and B. Hallet (2011), Denudation of the Namche Barwa antiform, eastern Himalaya, *Earth Planet. Sci. Lett.*, *307*, 323–333, doi:10.1016/j.epsl.2011.05.004.
Enkelmann, E., et al. (2015a), Cooperation among tectonic and surface processes in the St. Elias Range, Earth's highest coastal mountains, *Geophys. Res. Lett.*, *42*, 5838–5846, doi:10.1002/2015GL064727.
Enkelmann, E., P. G. Valla, and J.-D. Champagnac (2015b), Low-temperature thermochronology of the Yakutat plate corner, St. Elias Range (Alaska): Bridging short-term and long-term deformation, *Quat. Sci. Rev.*, *113*, 23–38, doi:10.1016/j.quascirev.2014.10.019.
Falkowski, S., E. Enkelmann, and T. A. Ehlers (2014), Constraining the area of rapid and deep-seated exhumation at the St. Elias syntaxis, southeast Alaska, with detrital zircon fission-track analysis, *Tectonics*, *33*, 597–616, doi:10.1002/2013TC003408.
Farley, K. A. (2000), Helium diffusion from apatite: General behavior as illustrated by Durango fluorapatite, *J. Geophys. Res.*, *105*, 2903–2914, doi:10.1029/1999JB900348.
Farley, K. A., R. A. Wolf, and L. T. Silver (1996), The effects of long alpha-stopping distances on U-Th/He dates, *Geochim. Cosmochim. Acta*, *60*, 4223–4230, doi:10.1016/S0016-7037(96)00193-7.
Farmer, G. L., R. Ayuso, and G. Plafker (1993), A Coast Mountains provenance for the Valdez and Orca groups, southern Alaska, based on Nd, Sr, and Pb isotopic evidence, *Earth Planet. Sci. Lett.*, *116*, 9–21, doi:10.1016/0012-821X(93)90042-8.
Ferris, A., G. A. Abers, D. H. Christensen, and E. Veenstra (2003), High resolution image of the subducted Pacific (?) Plate beneath central Alaska, 50–150 km depth, *Earth Planet. Sci. Lett.*, *214*, 575–588, doi:10.1016/S0012-821X(03)00403-5.
Finzel, E. S., J. M. Trop, K. D. Ridgway, and E. Enkelmann (2011), Upper plate proxies for flat-slab subduction processes in southern Alaska, *Earth Planet. Sci. Lett.*, *303*, 348–360, doi:10.1016/j.epsl.2011.01.014.
Fitzgerald, P. G., and J. W. Gleadow (1990), New approaches in fission track geochronology as a tectonic tool: Examples from the Transantarctic Mountains, *Int. J. Radiat. Appl. Instrum. Part D*, *17*, 351–357, doi:10.1016/1359-0189(90)90057-5.
Galbraith, R. F. (1981), On statistical models for fission track counts, *J. Int. Assoc. Math. Geol.*, *13*, 471–478, doi:10.1007/BF01034498.
Galbraith, R. F. (2005), *Interdisciplinary Statistics, Statistics for Fission Track Analysis*, 219 pp., Chapman Hall CRC Taylor Francis Group, Boca Raton, Fla.
Gardner, M. C., S. C. Bergman, G. W. Cushing, E. M. MacKevett, G. Plafker, R. B. Campbell, C. J. Dodds, W. C. McClelland, and P. A. Mueller (1988), Pennsylvanian pluton stitching of Wrangellia and the Alexander Terrane, Wrangell Mountains, Alaska, *Geology*, *16*, 967–971, doi:10.1130/0091-7613(1988)016<0967:PPSOWA>2.3.CO;2.
Garver, J. I., and C. M. Davidson (2015), Southwestern Laurentian zircons in Upper Cretaceous flysch of the Chugach-Prince William terrane in Alaska, *Am. J. Sci.*, *315*, 537–556, doi:10.2475/06.2015.02.
Gasser, D., E. Bruand, K. Stüwe, D. A. Foster, R. Schuster, B. Fügenschuh, and T. L. Pavlis (2011), Formation of a metamorphic complex along an obliquely convergent margin: Structural and thermochronological evolution of the Chugach Metamorphic Complex, southern Alaska, *Tectonics*, *30*, TC2012, doi:10.1029/2010TC002776.
Gasser, D., D. Rubatto, E. Bruand, and K. Stüwe (2012), Large-scale, short-lived metamorphism, deformation, and magmatism in the Chugach Metamorphic Complex, southern Alaska: A SHRIMP U-Pb study of zircon, *Geol. Soc. Am. Bull.*, *124*, 886–905, doi:10.1130/B30507.1.
Gehrels, G. E., et al. (2009), U-Th-Pb geochronology of the Coast Mountains batholith in north-coastal British Columbia: Constraints on age and tectonic evolution, *Geol. Soc. Am. Bull.*, *121*, 1341–1361, doi:10.1130/B26404.1.
Gleadow, A. J., and I. R. Duddy (1981), A natural long-term track annealing experiment for apatite, *Nucl. Tracks*, *5*, 169–174, doi:10.1016/0191-278X(81)90039-1.
Grabowski, D. M., E. Enkelmann, and T. A. Ehlers (2013), Spatial extent of rapid denudation in the glaciated St. Elias syntaxis region, SE Alaska, *J. Geophys. Res. Earth Surf.*, *118*, 1921–1938, doi:10.1002/jgrf.20136.
Gulick, S. P., L. A. Lowe, T. L. Pavlis, J. V. Gardner, and L. A. Mayer (2007), Geophysical insights into the Transition Fault debate: Propagating strike slip in response to stalling Yakutat block subduction in the Gulf of Alaska, *Geology*, *35*, 763–766, doi:10.1130/G2358A.1.
Gulick, S. P., et al. (2015), Mid-Pleistocene climate transition drives net mass loss from rapidly uplifting St. Elias Mountains, Alaska, *Proc. Natl. Acad. Sci. U.S.A.*, *112*, 15,042–15,047, doi:10.1073/pnas.1512549112.
Haeussler, P. J., G. E. Gehrels, and S. M. Karl (2005), Constraints on the age and provenance of the Chugach Accretionary Complex from detrital zircons in the Sitka Graywacke near Sitka, Alaska, in Studies by the U.S. Geol. Surv. in Alaska, 2004, *U.S. Geol. Surv. Prof. Pap.*, *1709-F*.
Hallet, B., L. Hunter, and J. Bogen (1996), Rates of erosion and sediment evacuation by glaciers: A review of field data and their implications, *Global Planet. Change*, *12*, 213–235, doi:10.1016/0921-8181(95)00021-6.
Harrison, T. M. (1982), Diffusion of ^{40}Ar in hornblende, *Contrib. Mineral. Petrol.*, *78*(3), 324–331, doi:10.1007/BF00398927.
Harrison, T. M., I. Duncan, and I. McDougall (1985), Diffusion of ^{40}Ar in biotite: Temperature, pressure and compositional effects, *Geochim. Cosmochim. Acta*, *49*, 2461–2468, doi:10.1016/0016-7037(85)90246-7.
Headley, R. M., E. Enkelmann, and B. Hallet (2013), Examination of the interplay between glacial processes and exhumation in the Saint Elias Mountains, Alaska, *Geosphere*, *9*, 229–241, doi:10.1130/GES00810.1.
Hillhouse, J. W. (1977), Paleomagnetism of the Triassic Nikolai Greenstone, McCarthy Quadrangle, Alaska, *Can. J. Earth Sci.*, *14*, 2578–2592, doi:10.1139/e77-223.
Hudson, T., G. Plafker, and M. A. Lanphere (1977a), Intrusive rocks of the Yakutat-St. Elias area, south-central Alaska, *J. Res. U. S. Geol. Surv.*, *5*, 155–172.
Hudson, T., G. Plafker, and D. L. Turner (1977b), Metamorphic rocks of the Yakutat-St. Elias area, south-central Alaska, *J. Res. U. S. Geol. Surv.*, *5*, 173–184.
Hudson, T., G. Plafker, and Z. E. Peterman (1979), Paleogene anatexis along the Gulf of Alaska margin, *Geology*, *7*, 573–577, doi:10.1130/0091-7613(1979)7<573:PAATGO>2.0.CO;2.
Israel, S. (2004), Geology of southwestern Yukon, Yukon Geological Survey open file 2004-16, scale 1:250000, Yukon Geological Survey, Whitehorse, Yukon.
Jaeger, J. M., C. A. Nittrouer, N. D. Scott, and J. D. Milliman (1998), Sediment accumulation along a glacially impacted mountainous coastline: North-east Gulf of Alaska, *Basin Res.*, *10*, 155–173, doi:10.1046/j.1365-2117.1998.00059.x.

Jones, D. L., N. J. Silberling, and J. Hillhouse (1977), Wrangellia—A displaced terrane in northwestern North America, *Can. J. Earth Sci.*, *14*, 2565–2577, doi:10.1139/e77-222.
Kochelek, E. J., J. M. Amato, T. L. Pavlis, and P. D. Clift (2011), Flysch deposition and preservation of coherent bedding in an accretionary complex: Detrital zircon ages from the Upper Cretaceous Valdez Group, Chugach Terrane, Alaska, *Lithosphere*, *3*, 265–274, doi:10.1130/L131.1.
Koons, P. O., B. P. Hooks, T. L. Pavlis, P. Upton, and A. D. Barker (2010), Three-dimensional mechanics of Yakutat convergence in the southern Alaskan plate corner, *Tectonics*, *29*, TC4008, doi:10.1029/2009TC002463.
Koons, P. O., P. K. Zeitler, and B. Hallet (2013), Tectonic aneurysms and mountain building, in *Treatise on Geomorphology*, *Tectonic Geomorphology*, vol. 5, edited by J. Shroder and L. A. Owen, pp. 318–349, Academic Press, San Diego, Calif.
Kretz, R. (1983), Symbols for rock-forming minerals, *Am. Mineral.*, *68*, 277–279.
Lagoe, M. B., and S. D. Zellers (1996), Depositional and microfaunal response to Pliocene climate change and tectonics in the eastern Gulf of Alaska, *Mar. Micropaleontol.*, *27*, 121–140, doi:10.1016/0377-8398(95)00055-0.
Lagoe, M. B., C. H. Eyles, N. Eyles, and C. Hale (1993), Timing of Late Cenozoic tidewater glaciation in the far North Pacific, *Geol. Soc. Am. Bull.*, *105*, 1542–1560, doi:10.1130/0016-7606(1993)105<1542:TOLCTG>2.3.CO;2.
Loney, R. A., and G. R. Himmelberg (1983), Structure and petrology of the La Perouse gabbro intrusion, Fairweather Range, southeastern Alaska, *J. Petrol.*, *24*, 377–423, doi:10.1093/petrology/24.4.377.
Loney, R. A., D. A. Brew, L. J. Muffler, and J. S. Pomeroy (1975), Reconnaissance geology of Chichagof, Baranof, and Kruzof Islands, Alaska, *U.S. Geol. Surv. Prof. Pap.*, *792*, 105 p.
Marechal, A., S. Mazzotti, J. L. Elliott, J. T. Freymueller, and M. Schmidt (2015), Indentor-corner tectonics in the Yakutat-St. Elias collision constrained by GPS, *J. Geophys. Res. Solid Earth*, *120*, 3897–3908, doi:10.1002/2014JB011842.
Mazzotti, S., and R. D. Hyndman (2002), Yakutat collision and strain transfer across the northern Canadian Cordillera, *Geology*, *30*, 495–498, doi:10.1130/0091-7613(2002)030<0495:YCASTA>2.0.CO;2.
McAleer, R. J., J. A. Spotila, E. Enkelmann, and A. L. Berger (2009), Exhumation along the Fairweather Fault, southeastern Alaska, based on low-temperature thermochronometry, *Tectonics*, *28*, TC1007, doi:10.1029/2007TC002240.
Meigs, A. J., S. Johnston, J. I. Garver, and J. A. Spotila (2008), Crustal-scale structural architecture, shortening, and exhumation of an active, eroding orogenic wedge (Chugach/St. Elias Range, southern Alaska), *Tectonics*, *27*, TC4003, doi:10.1029/2007TC002168.
Mezger, K., and E. J. Krogstad (1997), Interpretation of discordant U-Pb zircon ages: An evaluation, *J. Metamorph. Geol.*, *15*, 127–140, doi:10.1111/j.1525-1314.1997.00008.x.
Molnia, B. F. (2008), Glaciers of North America: Glaciers of Alaska, in *Satellite Image Atlas of Glaciers of the World*, *U.S. Geol. Surv. Prof. Pap., 1386-K*, edited by R. S. Williams Jr. and J. G. Ferrigno, 521 pp., U.S. Geol. Surv., Washington, D. C.
Nokleberg, W. J., G. Plafker, and F. H. Wilson (1994), Geology of south-central Alaska, in *The Geology of Alaska*, *The Geol. of North America*, vol. G-1, edited by G. Plafker and H. C. Berg, pp. 311–366, GSA, Boulder, Colo.
O'Sullivan, P. B., and L. D. Currie (1996), Thermotectonic history of Mt. Logan, Yukon Territory, Canada: Implications of multiple episodes of Middle to Late Cenozoic denudation, *Earth Planet. Sci. Lett.*, *144*, 251–261, doi:10.1016/0012-821X(96)00161-6.
O'Sullivan, P. B., G. Plafker, and J. M. Murphy (1997), Apatite fission-track thermotectonic history of crystalline rocks in the northern Saint Elias Mountains, Alaska, in *The United States Geological Survey in Alaska*, *U.S. Geol. Surv. Prof. Pap., 1574*, edited by J. A. Dumoulin and J. E. Gray, pp. 283–294, Denver, Colo.
Pavlis, T. L., and V. B. Sisson (1995), Structural history of the Chugach metamorphic complex in the Tana River region, eastern Alaska: A record of Eocene ridge subduction, *Geol. Soc. Am. Bull.*, *7*, 1333–1355, doi:10.1130/0016-7606(1995)107<1333:SHOTCM>2.3.CO;2.
Pavlis, T. L., C. Picornell, and L. Serpa (2004), Tectonic processes during oblique collision: Insights from the St. Elias orogen, northern North American Cordillera, *Tectonics*, *23*, TC3001, doi:10.1029/2003TC001557.
Pavlis, T. L., J. B. Chapman, R. L. Bruhn, K. Ridgway, L. L. Worthington, S. P. Gulick, and J. Spotila (2012), Structure of the actively deforming fold-thrust belt of the St. Elias orogen with implications for glacial exhumation and three-dimensional tectonic processes, *Geosphere*, *8*, 991–1019, doi:10.1130/GES00753.1.
Perry, S. E., J. I. Garver, and K. D. Ridgway (2009), Transport of the Yakutat Terrane, southern Alaska: Evidence from sediment petrology and detrital zircon fission-track and U/Pb double dating, *J. Geol.*, *117*, 156–173, doi:10.1086/596302.
Plafker, G. (1987), Regional geology and petroleum potential of the northern Gulf of Alaska continental margin, in *Geology and Resource Potential of the Continental Margin of Western North America and Adjacent Ocean Basins*, *Earth Science Ser.*, vol. 6, edited by D. W. Scholl et al., pp. 229–268, Circum Pacific Counc. for Energy and Miner. Resources, Houston, Tex.
Plafker, G., and E. M. MacKevett (1969), Mafic and ultramafic rocks from a layered pluton at Mount Fairweather, Alaska, in *Geological Survey Research 1970*, *U.S. Geol. Surv. Prof. Pap., 700-B*, pp. B21–B26, Washington, D. C.
Plafker, G., W. J. Nokleberg, and J. S. Lull (1989), Bedrock geology and tectonic evolution of the Wrangellia, Peninsular, and Chugach Terranes along the Trans-Alaskan Crustal Transect in the Chugach Mountains and southern Copper River Basin, Alaska, *J. Geophys. Res.*, *94*, 4255–4295, doi:10.1029/JB094iB04p04255.
Plafker, G., J. C. Moore, and G. R. Winkler (1994), Geology of the southern Alaska margin, in *The Geology of North America*, *The Geol. of Alaska*, vol. G-1, edited by G. Plafker and H. C. Berg, pp. 389–449, GSA, Boulder, Colo.
Plattner, C., R. Malservisi, T. H. Dixon, P. LaFemina, G. F. Sella, J. Fletcher, and F. Suarez-Vidal (2007), New constraints on relative motion between the Pacific Plate and Baja California microplate (Mexico) from GPS measurements, *Geophys. J. Int.*, *170*, 1373–1380, doi:10.1111/j.1365-246X.2007.03494.x.
Rahn, M. K., M. T. Brandon, G. E. Batt, and J. I. Garver (2004), A zero-damage model for fission-track annealing in zircon, *Am. Mineral.*, *89*, 473–484, doi:10.2138/am-2004-0401.
Reiners, P. W., and M. T. Brandon (2006), Using thermochronology to understand orogenic erosion, *Annu. Rev. Earth Planet. Sci.*, *34*, 419–466, doi:10.1146/annurev.earth.34.031405.125202.
Reiners, P. W., T. L. Spell, S. Nicolescu, and K. A. Zanetti (2004), Zircon (U-Th)/He thermochronometry: He diffusion and comparison with $^{40}Ar/^{39}Ar$ dating, *Geochim. Cosmochim. Acta*, *68*, 1857–1887, doi:10.1016/j.gca.2003.10.021.
Richter, D. H., J. G. Smith, M. A. Lanphere, G. B. Dalyrmple, G. B. Reed, and N. B. Shew (1990), Age and progression of volcanism, Wrangell volcanic field, Alaska, *Bull. Volcanol.*, *53*, 29–44, doi:10.1007/BF00680318.
Richter, D. H., C. C. Preller, K. A. Labay, and N. B. Shew (2006), Geologic map of the Wrangell-St. Elias National Park and Preserve, Alaska, Scientific investigations map 2877, scale 1:350000, U.S. Geol. Surv.
Rick, B. J., B. K. Frett, C. M. Davidson, and J. I. Garver (2014), U/Pb dating of detrital zircon from Seward to Baranof Island provides depositional links across the Chugach-Prince William Terrane in southeastern Alaska, Cordilleran Tectonics Workshop, UBC Okanagan, Abstracts, 35–36.

Rignot, E., J. Mouginot, C. F. Larsen, Y. Gim, and D. Kirchner (2013), Low-frequency radar sounding of temperate ice masses in Southern Alaska, *Geophys. Res. Lett.*, *40*, 5399–5405, doi:10.1002/2013GL057452.

Roeske, S. M., L. W. Snee, and T. L. Pavlis (2003), Dextral-slip reactivation of an arc-forearc boundary during Late Cretaceous–Early Eocene oblique convergence in the northern Cordillera, *Geol. Soc. Am. Spec. Pap.*, *371*, 141–169, doi:10.1130/0-8137-2371-X.29.

Rossman, D. L. (1963), Geology and petrology of two stocks of layered gabbro in the Fairweather Range, Alaska, *U.S. Geol. Surv. Bull. 1121-F*, 50 p.

Sheaf, M. A., L. Serpa, and T. L. Pavlis (2003), Exhumation rates in the St. Elias Mountains, Alaska, *Tectonophysics*, *367*, 1–11, doi:10.1016/S0040-1951(03)00124-0.

Sisson, V. B., and L. S. Hollister (1988), Low-pressure facies series metamorphism in an accretionary sedimentary prism, southern Alaska, *Geology*, *16*, 358–361, doi:10.1130/0091-7613(1988)016<0358:LPFSMI>2.3.CO;2.

Sisson, V. B., A. R. Poole, N. R. Harris, H. C. Burner, T. L. Pavlis, P. Copeland, R. A. Donelick, and W. C. McClelland (2003), Geochemical and geochronologic constraints for genesis of a tonalite-trondhjemite suite and associated mafic intrusive rocks in the eastern Chugach Mountains, Alaska: A record of ridge-transform subduction, *Geol. Soc. Am. Spec. Pap.*, *371*, 293–326, doi:10.1130/0-8137-2371-X.29.

Smart, K. J., T. L. Pavlis, V. B. Sisson, S. M. Roeske, and L. W. Snee (1996), The Border Ranges fault system in Glacier Bay National Park, Alaska—Evidence for major early Cenozoic dextral strike-slip motion, *Can. J. Earth Sci.*, *33*, 1268–1282, doi:10.1139/e96-096.

Spotila, J. A., and A. L. Berger (2010), Exhumation at orogenic indentor corner under long-term glacial conditions: Example of the St. Elias orogen, southern Alaska, *Tectonophysics*, *490*, 241–256, doi:10.1016/j.tecto.2010.05.015.

Spotila, J. A., J. T. Buscher, A. J. Meigs, and P. W. Reiners (2004), Long-term glacial erosion of active mountain belts, Example of the Chugach-St. Elias Range, Alaska, *Geology*, *32*, 501–504, doi:10.1130/G20343.1.

Suess, E. (1904), *The Face of the Earth (Das Antlitz der Erde)*, vol. 1, 604 pp., Clarendon Press, Oxford, U. K.

Tagami, T., A. Carter, and A. J. Hurford (1996), Natural long-term annealing of the zircon fission-track system in Vienna Basin deep borehole samples: Constraints upon the partial annealing zone and closure temperature, *Chem. Geol.*, *130*, 147–157, doi:10.1016/0009-2541(96)00016-2.

Trop, J. M., K. D. Ridgway, J. D. Manuszak, and P. Layer (2002), Mesozoic sedimentary-basin development on the allochthonous Wrangellia Composite Terrane, Wrangell Mountains Basin, Alaska: A long-term record of terrane migration and arc construction, *Geol. Soc. Am. Bull.*, *114*, 693–717, doi:10.1130/0016-7606(2002)114<0693:MSBDOT>2.0.CO;2.

White, J. M., T. A. Ager, D. P. Adam, E. B. Leopold, G. Liu, H. Jetté, and C. E. Schweger (1997), An 18 million year record of vegetation and climate change in northwestern Canada and Alaska: Tectonic and global climatic correlates, *Palaeogeogr. Palaeoclimatol. Palaeoecol.*, *130*, 293–306, doi:10.1016/S0031-0182(96)00146-0.

Worthington, L. L., S. P. Gulick, and T. L. Pavlis (2010), Coupled stratigraphic and structural evolution of a glaciated orogenic wedge, *Tectonics*, *29*, TC6013, doi:10.1029/2010TC002723.

Worthington, L. L., H. J. Van Avendonk, S. P. Gulick, G. L. Christeson, and T. L. Pavlis (2012), Crustal structure of the Yakutat Terrane and the evolution of subduction and collision in southern Alaska, *J. Geophys. Res.*, *117*, B01102, doi:10.1029/2011JB008493.

Zeitler, P. K., J. F. Sutter, I. Williams, R. E. Zartman, and R. A. Tahirkheli (1989), Geochronology and temperature history of the Nanga Parbat–Haramosh Massif, Pakistan, *Geol. Soc. Am. Spec. Pap.*, *232*, 1–22, doi:10.1130/SPE232–p1.

Zeitler, P. K., et al. (2001), Erosion, Himalayan geodynamics, and the geomorphology of metamorphism, *GSA Today*, *11*, 4–9, doi:10.1130/1052-5173(2001)011<0004:EHGATG>2.0.CO;2.

Zeitler, P. K., A. S. Meltzer, L. Brown, W. S. Kidd, C. Lim, and E. Enkelmann (2014), Tectonics and topographic evolution of Namche Barwa and the easternmost Lhasa block, Tibet, *Geol. Soc. Am. Spec. Pap.*, *507*, 23–58, doi:10.1130/2014.2507(02).